A Position Controller for Hydraulic Excavators with Deadtime and Regenerative Pipelines

Yuki Yamamoto[1,2,*], Jinjun Qiu[3], Takayuki Doi[3],
Takao Nanjo[3], Koji Yamashita[3], and Ryo Kikuuwe[1]

***Abstract*—This paper proposes a position controller for commercial hydraulic excavators. It is constructed by combining a proportional-derivative (PD) controller and a sliding-mode controller as a differential algebraic inclusion and also is integrated with a recently-proposed hydraulic actuator model. The use of the PD control is intended to make the controller insensitive to the deadtime in the hydraulic system, which is typically 0.1 s to 0.6 s in commercial excavators. The use of the sliding-mode controller combined with the actuator model is for handling the saturation of the actuator force, which may happen when the target position is not close enough to the current position and when the relief valves open. Moreover, this paper extends the controller to deal with the effect of the regenerative pipelines, which are embedded in commercial excavators to realize efficient operations but act as a source of disturbance on the controller. This paper also shows an analysis that can be used for tuning the controller parameters. The proposed controller was validated with simulations and experiments using a 13-ton class excavator, in which some set-point control tasks and trajectory-tracking tasks were performed.**

***Note to Practitioners*—This paper proposes a position controller for hydraulic excavators. The controller was validated with the boom and arm actuators of a 13-ton class commercial excavator, with trajectory-tracking and set-point control tasks. Most of the controller parameters can be set referring to available specifications of the hydraulic circuit, such as the set pressures of the relief valves and the cross-sectional areas of the chambers. There are three parameters (the proportional gain, the derivative gain, and the time constant of the convergence) that should be carefully tuned, but their physical interpretations are relatively straightforward, and they can also be tuned along our guideline using pole locations of a particular transfer function. It has been shown that the proposed controller properly works despite the existence of the deadtime in the hydraulic systems, which are typically 0.1 s to 0.6 s. An extended version of the proposed controller handles the effects of the regenerative pipeline, which exists in some hydraulic systems, e.g., the arm actuator, for efficient operation and is not accounted for in the original version of the controller. The accuracy of the proposed controller will be further improved by combining it with better means to estimate external forces by using additional sensors, such as pressure sensors installed to actuator chambers.**

***Index Terms*—Position control, Hydraulic systems, Time delay.**

*Corresponding author (e-mail: y.yamamoto@mdl.hiroshima-u.ac.jp)
[1]Machinery Dynamics Laboratory, Hiroshima University, 1-4-1 Kagamiyama, Higashi-Hiroshima, Hiroshima 739-8527, Japan
[2]Research Fellow of Japan Society for the Promotion of Science
[3]Kobelco Construction Machinery Co., Ltd., 2-2-1 Itsukaichiko, Saeki-ku, Hiroshima 731-5161, Japan
This work was supported by Kobelco Construction Machinery Co., Ltd.

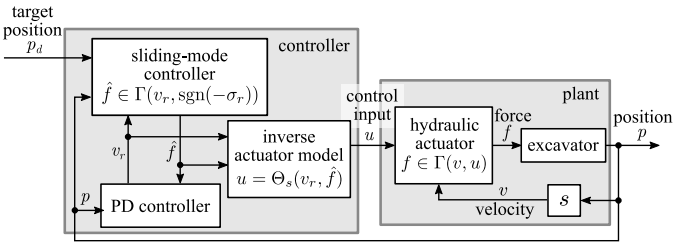

Fig. 1. Block diagram of the proposed controller, where v_r is a reference velocity, $\hat{f}$ is the intended actuator force, and u is the control input to determine the opening ratios of the main control valves. The functions Γ and Θ describe the quasistatic relation among the force f, the velocity v, and the control input u, as detailed in Section II-C. The sliding surface is $\sigma_r \triangleq p - p_d + H(v_r - \dot{p}_d) = 0$.

I. Introduction

Position control technology for hydraulic excavators is a prerequisite for future automation in construction sites. The actuators used in commercial excavators are composed of many valves and pipelines, which cause strong nonlinearity in the response characteristics of the actuators. Specifically, the check valves and the relief valves in the hydraulic circuit act as on-off switches of the oil flow, and thus result in non-differentiability or discontinuity in the velocity-force and flowrate-pressure relations. Such features of hydraulic systems pose difficulty in the control of excavators.

One approach for the control of hydraulic systems is employing a locally linearized model of the system. Some controllers [1]–[4] with linearized models are reported to achieve tracking tasks with smooth position commands. Another approach is combining gain-tuning methods with linear controllers [5]–[8] in which the control gains are optimized in metaheuristic algorithms. Some researchers [9]–[13] employ neural networks to approximate the actuator characteristics, but the actuator force saturation, which frequently happens and discontinuously alters the response characteristics, has not been taken into account.

Another problematic factor in the control of hydraulic systems is the deadtime, which is typically 0.1 s to 0.6 s or more [2], [4], [14] in commercial hydraulic excavators. There have been some controllers based on models of the deadtime in hydraulic systems [2], [4], [11], [12], but they require the identification of the deadtime, and the control performance depends on the precision of the identification.

Recently, the authors proposed a set-point position controller [14] for hydraulic excavators. It fully considers the circuit structure, composed of various valves and pipelines,

by employing a quasistatic actuator model [15]. It can be seen as a particular type of a sliding-mode controller combined with a deadtime compensation based on the dynamics model of the excavator. Its biggest problem is that its control performance highly depends on the accuracy of the state prediction, employing the plant dynamics model, for the deadtime compensation.

This paper proposes yet another position controller for hydraulic actuators that is also a sliding-mode-like controller but is free from explicit compensation for the deadtime. The motivation for the controller design is to avoid measuring the exact length of the deadtime, which is usually difficult in real-world applications. The controller has a structure illustrated in Fig. 1. It is a differential-algebraic combination of a sliding-mode controller and a proportional-derivative (PD) controller, and employs the quasistatic actuator model [15] to determine the control input. The use of the PD controller is to realize a certain level of robustness against the deadtime by tuning the gains (cf., e.g., [16, Chapter 4]). The intention for employing a sliding-mode-like controller is to explicitly cope with the force saturations, which is somewhat different from a common aim of using sliding modes to ensure accurate convergence [1], [13], [17], [18]. In addition, the controller is extended to handle a regenerative pipeline in the hydraulic circuit, which is not explicitly taken into account in the quasistatic actuator model.

One novelty of the proposed controller is the combination of a PD controller and a sliding-mode controller with a hydraulic actuator model [15]. Some robot controllers proposed by Kikuuwe [19], [20] have also been built on the same idea, but these controller mainly focus on electromagnetic actuators, which do not require elaborate actuator models. Another novelty of the proposed controller is that it fully takes into account the effects of regenerative pipelines and other valves.

The rest of this paper is organized as follows. Section II provides some preliminaries regarding set-valued functions, related work, the quasistatic actuator model [15], and the authors' previous controller [14]. Section III presents the proposed position controller and its discrete-time algorithm. Section IV provides some analyses on the controller. Sections V and VI show the results of simulations and experiments employing a 13-ton class excavator, respectively. Section VII concludes this paper.

II. Preliminaries

A. Mathematical Preliminaries

In this paper, $\mathbb{R}$ denotes the set of all real numbers and $\mathcal{B}$ denotes the closed unit ball in $\mathbb{R}$, i.e., $\mathcal{B} \triangleq [-1, 1] \subset \mathbb{R}$.

The following functions are used in this paper:

$$\mathrm{sat}_{\mathcal{X}}(x) \triangleq \begin{cases} \min \mathcal{X} & \text{if } x < \min \mathcal{X} \\ x & \text{if } x \in \mathcal{X} \\ \max \mathcal{X} & \text{if } x > \max \mathcal{X} \end{cases} \tag{1}$$

$$\mathrm{sgn}(x) \triangleq \begin{cases} x/|x| & \text{if } x \neq 0 \\ [-1, 1] & \text{if } x = 0 \end{cases} \tag{2}$$

$$\mathcal{R}(x) \triangleq \mathrm{sgn}(x)\sqrt{|x|}. \tag{3}$$

In addition, a function of a set should be understood in the following manner:

$$\Phi(\mathcal{X}) = \bigcup_{x \in \mathcal{X}} \Phi(x). \tag{4}$$

Here, $\mathcal{X}$ is a closed interval in $\mathbb{R}$. The function $\mathcal{R}$, which also appears in our previous papers [14], [15], is used to concisely describe the square-root relations [21] between the flowrates and the pressures across valves.

B. Related Work

Several controllers [1]–[4] for hydraulic excavators have been proposed based on a locally linearized model of the system. Some of the controllers [1]–[3] are based on a time-delay-control approach, in which the uncertain dynamics of the plant are estimated from the measured states, such as actuator torques and joint angles. Kim et al. [4] designed a robust controller based on μ-synthesis with as a second-order plus deadtime model of the plant. Gain-tuning methods [5]–[8] based on metaheuristic approaches, such as particle swarm optimization and genetic algorithms, have been proposed for linear controllers. To handle the strong nonlinearity of the actuator characteristics, some controllers [9]–[13] employ neural networks for the compensation of the nonlinearity. It has been reported that smooth trajectory tracking can be achieved with these controllers, but no controller analytically takes into account the valve effects, such as the force saturation and the square-root law [21] of the pressure-flowrate relation.

It has been reported that the hydraulic systems have large deadtime, which is typically 0.1 s to 0.6 s or more [2], [4], [14] in commercial hydraulic excavators. Kim et al. [4] modeled a hydraulic plant as a second-order system with a deadtime, which is measured in preliminary experiments, and designed a position controller based on the model. Chang et al. [2] proposed a position controller with an additional linear controller based on chamber pressures to compensate for the deadtime. There are learning-based controllers for hydraulic excavators with deadtime [11], [12]. Lee et al. [11] proposed a motion controller based on a data-driven model of the excavators. Egli et al. [12] proposed a control approach employing reinforcement learning for excavators with the deadtime. These controllers, which explicitly compensate for the deadtime, achieve accurate trajectory tracking, but their performance depends on the accuracy of the learning and the identification of the actuator dynamics including the deadtime.

Some hydraulic actuators in excavators have auxiliary pipelines known as regenerative pipelines for enhancing task efficiency. These pipelines inject additional complexities to the actuator characteristics. An example of work involving regenerative pipelines is the study by Kim et al. [22]. They proposed a velocity-field controller based on a detailed model of actuators with regenerative pipelines, but it does not take into account the saturation of the actuator force.

The aforementioned controllers can handle either valve effects, deadtime or regenerative pipelines, but as far as the authors are aware, there is no controller that can handle all of them.

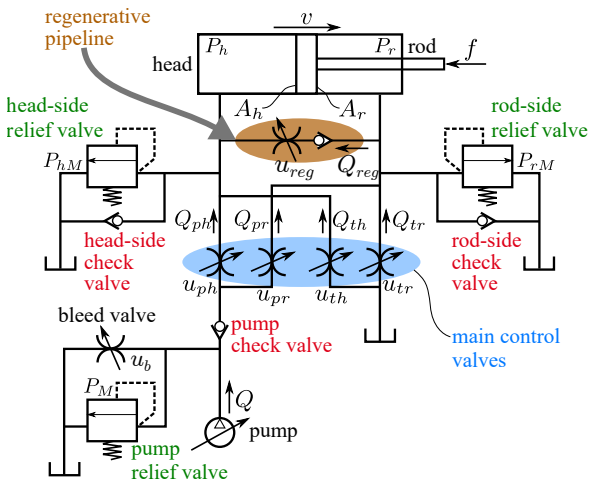

Fig. 2. Hydraulic actuator and its circuit. It is close to the one considered in [14] but the regenerative pipeline is now included.

C. Quasistatic Actuator Model

The overall structure of the actuator considered in this paper is illustrated in Fig. 2. As can be seen in the figure, the circuit has a pump, which supplies the oil in the circuit at a flowrate Q. In order to control the hydraulic flow, the circuit is equipped with four main control valves and a bleed valve. The head-side, rod-side, and pump relief valves are for securing the oil outlet, of which the pressure limits are P_{hM}, P_{rM}, and P_M, respectively. This circuit has three check valves to prevent the backflow of the oil. The actuator is divided into two chambers by a piston, of which cross-sectional areas and internal pressures are denoted by A_* and P_* ($* \in \{h, r\}$), respectively (where h means head-side and r means rod-side). The actuator force is lower-bounded by $-F_{rM} \triangleq -A_r P_{rM}$ and upper-bounded by $F_{hM} \triangleq A_h P_{hM}$ due to the effects of the head-side and rod-side relief valves.

The ratio of the opening area to its maximum of each of five control valves (four main control valves and the bleed valve) is denoted by $u_* \in [0, 1]$ ($* \in \{ph, pr, th, tr, b\}$). The flowrates Q_* of the valves satisfy the following flowrate-pressure relations [21], [23]:

$$Q_* = c_* u_* \mathcal{R}(\Delta P_*) \ (* \in \{ph, tr, th, pr, b\}) \tag{5}$$

where $c_* \triangleq C_* a_* \sqrt{2/\rho}$, ΔP_* is the pressure drop across the valve, ρ is the mass density of the oil, a_* is the maximum opening area of the valve, and C_* is its discharge coefficient [24], which is a non-dimensional quantity. It has been known [25], [26] that C_* is typically around 0.6 or 0.7.

The actuators of excavators may have an additional pipeline, referred to as the regenerative pipeline, which is also included in the diagram of Fig. 2. This pipeline is for making the extending motion faster when the actuator is subjected to the tensile external force. Typically, excavators' arm actuators (as opposed to the boom or bucket actuators) possess this architecture to accelerate the arm lowering action. The flowrate through the regenerative pipeline Q_{reg} can be given as follows:

$$Q_{reg} = c_{reg} u_{reg} \max(\mathcal{R}(P_r - P_h), 0) \tag{6}$$

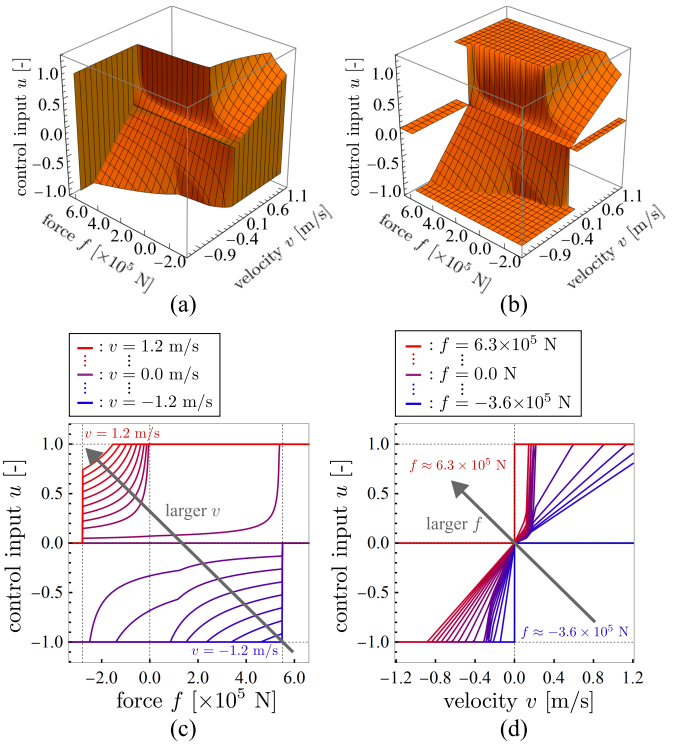

Fig. 3. Graphs of $u \in \Theta(v, f)$ and $u = \Theta_s(v, f)$ representing the actuator model [14], [15], where the control input u determines the opening ratios of the main control valves through (8). (a) Graph of $u \in \Theta(v, f)$ in the v-f-u space. (b) Graph of $u = \Theta_s(v, f)$ in the v-f-u space. (c) Cross-sections of (b) at different velocities $v \in [-1.2 \text{ m/s}, 1.2 \text{ m/s}]$, which are indicated by the line colors ranging from blue to red. (d) Cross-sections of (b) at different forces $f \in [-3.6{\times}10^5 \text{ N}, 6.3{\times}10^5 \text{ N}]$, which are indicated by the line colors ranging from blue to red.

where $c_{reg} \triangleq C_{reg} a_{reg} \sqrt{2/\rho}$, u_{reg} denotes the ratio of the opening area to its maximum, a_{reg} is the maximum opening area of the valve, and C_{reg} is the discharge coefficient [24] of the valve.

Let us now focus on the actuator illustrated in Fig.2 with the regenerative pipeline being excluded. The previous study [15] presented a quasistatic model of such an actuator. The model is represented by a set-valued function Γ that connects the actuator force $f \in \mathbb{R}$, the rod velocity $v \in \mathbb{R}$, and the control input $u \in \mathcal{B}$ in the following form:

$$f \in \Gamma(v, u). \tag{7}$$

Here, the control input u means the signal that determines the valve opening ratios in the following manner:

$$u_{ph} = u_{tr} = \max(0, u), \ u_{pt} = u_{th} = -\min(0, u). \tag{8}$$

Note that the control input $u \in \mathcal{B}$ is not to be confused with the valve opening ratios $u_* \in [0, 1]$ ($* \in \{ph, tr, pt, th\}$). The exact analytical form of the set-valued function Γ is presented in [15].

For the use of the model in control and simulation, the function Γ needs to be transformed into some different forms. First, as detailed in [27], we need to have the inverse function Θ of the function Γ with respect to its second argument, which satisfies the following:

$$u \in \Theta(v, f) \iff f \in \Gamma(v, u). \tag{9}$$

Here, note that Θ is also a set-valued function. In addition, we need two single-valued functions Θ_s and Γ_s, which satisfy the following relations:

$$f = \Gamma_s(\eta, v, u) \iff f \in \Gamma(v + \eta f, u) \tag{10}$$

$$\Theta_s(v, f) \in \Theta\left(v, \mathrm{sat}_{\Gamma(v,\mathcal{B})}(f)\right) \tag{11}$$

where $\eta > 0$. The analytical forms of the functions Γ_s, Θ_s, and Θ are provided in [14] and [27, Theorem 3]. Fig. 3 shows graphs of Θ_s with the parameter values of the boom actuator used in the simulations in Section V. As can be seen from Fig. 3(a), the function Θ is set-valued at $v = 0$, $f \approx 5.5{\times}10^5$ ($\approx F_{hM}$) or $f \approx -2.8{\times}10^5$ ($\approx -F_{rM}$). The function Θ_s can be seen as a single-valued and domain-extended version of the function Θ. A three-dimensional visualization of the function Θ is shown in Fig. 3(b), and Figs. 3(c) and (d) show the cross-sections in the v-u plane and the f-u plane, respectively. As seen in Figs. 3(c)(d), the control input u is monotone (monotonically increasing) with respect to v and f.

The circuit including the generative pipeline is also modeled in [15] in the quasistatic manner. The actuator model can be written in the following form:

$$f = F_h - F_r \tag{12a}$$

$$F_h \in \Gamma_h\left(v - Q_{reg}/A_h, u\right) \tag{12b}$$

$$F_r \in \Gamma_r\left(v - Q_{reg}/A_r, u\right) \tag{12c}$$

$$Q_{reg} = c_{reg} u_{reg} \max\left(\mathcal{R}\left(F_r/A_r - F_h/A_h\right), 0\right). \tag{12d}$$

Here, the functions Γ_h and Γ_r, which are detailed in [15], give the forces generated by the head- and rod-side chambers, respectively, and they satisfy $\Gamma(v, u) = \Gamma_h(v, u) - \Gamma_r(v, u)$. The quantities Q_{reg}, F_r, and F_h are determined by the algebraic constraints (12b), (12c), and (12d), and the algorithm of iterative computation to provide the solutions has been provided in [15]. This paper does not attempt to directly use it because of its high computational cost for the iterative computation. Instead, this paper uses an approximate, simplified form of the model inspired by the representation (12), which will be presented in Section III-D.

D. Previous Controller Using Quasistatic Actuator Model

In the previous paper [14], the authors proposed a set-point position controller for hydraulic excavator based on the quasistatic actuator model [15] overviewed in Section II-C. The controller was intended to be applied to the class of plants that are described as follows:

$$M\dot{v} = f + g \tag{13a}$$

$$\dot{p} = v \tag{13b}$$

$$f \in \Gamma(v, u) \tag{13c}$$

where $M > 0$ is the mass of the controlled object, $p \in \mathbb{R}$ and $v \in \mathbb{R}$ are the position and the velocity of the object, respectively, $f \in \mathbb{R}$ is the actuator force and $g \in \mathbb{R}$ is the external force acting to the object. The function Γ is the quasistatic actuator model discussed in Section II-C, and its second argument $u \in \mathcal{B}$ is the control input that should be given from a controller.

The previous controller [14] was constructed from the following continuous-time representation:

$$M\ddot{p} = \hat{f} + \hat{g} \tag{14a}$$

$$\hat{f} \in \Gamma\left(\dot{p}, \mathrm{sgn}(p_d - p - H(\dot{p}_d - \dot{p}))\right) \tag{14b}$$

$$u \in \Theta(v, f) \tag{14c}$$

where p_d is the target position, $\hat{g}$ is an estimated external force, $\hat{f}$ is an intended actuator force, and H is a parameter to determine the time constant of the convergence. Here, note that the equation (14a) is the nominal model of the controlled object (13a). The control input u is determined by an algorithm derived from the implicit-Euler discretization of (14) based on a mathematical framework detailed in [27].

To deal with the deadtime in the hydraulic actuator, the controller (14) in [14] was combined with a state predictor based on a nominal plant model, which is of the form of (13). It requires a predetermined look-ahead time $\hat{T}_d$, which should be set as close as possible to the deadtime, and the position and velocity of the time $\hat{T}_d$ future are predicted by the simple time integration of the nominal model of the form (13). The drawback of this approach is its strong dependency on the accuracy of the model, especially on the nominal inertia M.

III. Proposed Controller

A. Continuous-time Representation

This paper also intends to develop a controller for the class of plants described as (13). We propose a position controller whose continuous-time representation can be written as follows:

$$\hat{f} = K(p_r - p) + B(\dot{p}_r - \dot{p}) - \hat{g} \tag{15a}$$

$$\hat{f} \in \Gamma(\dot{p}_r, \mathrm{sgn}(p_d - p + H(\dot{p}_d - \dot{p}_r))) \tag{15b}$$

$$u \in \Theta(\dot{p}_r, \hat{f}). \tag{15c}$$

The inputs to the controller are the target position p_d, the measured position p, and the estimated external force $\hat{g}$. The output from the controller is the control input $u \in \mathcal{B}$. The controller possesses a state variable p_r, which can be seen as a reference position. The variable $\hat{f}$ can be interpreted as the intended actuator force, which is not a state variable but a function of the state variable and the inputs.

The main parts (15a) and (15b) of the controller constitute a set of differential-algebraic constraints that determines $\dot{p}_r$ and $\hat{f}$. This set of differential-algebraic constraints appears as an algebraic loop in the block diagram of Fig. 4. The obtained values are used in (15c) to determine the control input u. The controller algorithm to solve these constraints is derived through the implicit-Euler discretization as detailed in the next Section III-C.

In the proposed controller (15), the components (15a) and (15b) can be seen as a PD controller and a sliding-mode-like controller, respectively. The PD controller (15a), with the proportional gain of K and the derivative gain B, is intended to make the position p track the reference position p_r. The sliding-mode-like controller (15b) is to make the position p exponentially converge to the target position p_d with the time constant H.

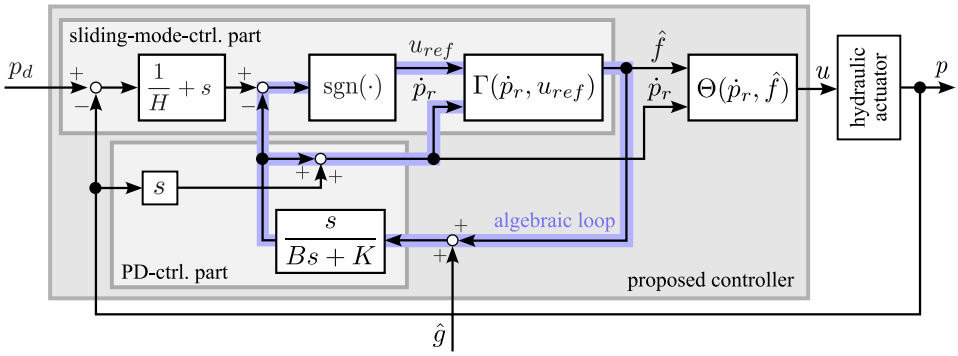

Fig. 4. Block diagram of the proposed controller. The set-valued functions Γ and Θ are determined according to the structure of the hydraulic circuit.

B. Properties of the Controller

Some properties of the controller (15) are now discussed. By setting $e \triangleq p_r - p$, we can rewrite (15) as follows:

$$\dot{e} = (\hat{f} + \hat{g} - Ke)/B \tag{16a}$$
$$\hat{f} \in \Gamma(\dot{p} + \dot{e}, \mathrm{sgn}(-\sigma/H - \dot{e})) \tag{16b}$$
$$u \in \Theta(\dot{p} + \dot{e}, \hat{f}) \tag{16c}$$

where $\sigma \triangleq p - p_d + H(\dot{p} - \dot{p}_d)$.

In the extreme case of $B \to \infty$, (16a) reduces to $\dot{e} = 0$, and thus the whole controller (16) reduces to the following:

$$u \in \Theta(\dot{p}, \Gamma(\dot{p}, \mathrm{sgn}(-\sigma/H))). \tag{17}$$

The controller (17) can be seen as a sliding mode controller with the sliding surface $\sigma = 0$, which is a variant of the one discussed in [27, Section IV.A].

Our previous controller [14], overviewed in Section II-D, was also derived from the sliding-mode controller (17), but it is algebraically combined with the plant dynamics model (14a). In contrast, the proposed controller is derived by combining (17) with the PD controller (15a). This difference is beneficial in that the proposed controller is less dependent on the plant dynamics model, which is not usually accurately available, and also in that the influence of the deadtime can be reduced to a certain level by appropriately tuning the PD gains, as has been discussed in, e.g., [16, Section 4.2]. It should be noted that the proposed controller does not incorporate explicit compensation for the deadtime, while the previous controller [14] required a deadtime compensation using a state predictor depending on a precalibrated look-ahead time $\hat{T}_d$.

Similar approaches combining a sliding-mode controller and a PD controller have been presented by Kikuuwe et al. [19], [20]. Their controllers are originally intended for mechatronics systems with electromagnetic actuators, to which the forces to be generated can be directly commanded. The very initial idea of the proposed controller was to combine the concept of Kikuuwe et al.'s [19] controller with the quasistatic model [15] of hydraulic actuators, but some modifications were needed to adapt it to the particular structure of the quasistatic actuator model [15]. Specifically, the sliding surface is approximated to $p_d - p_r + H(\dot{p}_d - \dot{p}_r) = 0$ in [19], while to $p_d - p + H(\dot{p}_d - \dot{p}_r) = 0$ in this paper. Because the proposed controller uses $\dot{p}_r$ as the first argument of Θ in (15c), $\dot{p}_r = 0$ results in $u = 0$. This means that the use of p_r in the sliding surface results in $u = 0$ when p_d is reached by p_r, not by p. This is the reason why the proposed controller uses the sliding surface comprising p, not p_r.

C. Discrete-time Implementation

Now we derive a discrete-time algorithm of the controller (15) through the implicit Euler discretization. For the convenience of derivation, let us rewrite (15) as follows:

$$\hat{f} = Ke + B\dot{e} - \hat{g} \tag{18a}$$
$$\hat{f} \in \Gamma(v_r, \mathrm{sgn}(p_d - p + H(v_d - v_r))) \tag{18b}$$
$$u \in \Theta(v_r, \hat{f}) \tag{18c}$$
$$\dot{e} = v_r - v, \quad \dot{p}_r = v_r, \quad \dot{p}_d = v_d. \tag{18d}$$

Its implicit Euler discretization can be obtained as follows:

$$\hat{f}_k = Ke_k + B(e_k - e_{k-1})/T - \hat{g}_k \tag{19a}$$
$$\hat{f}_k \in \Gamma(v_{r,k}, \mathrm{sgn}(p_{d,k} + Hv_{d,k} - p_k - Hv_{r,k})) \tag{19b}$$
$$u_k \in \Theta(v_{r,k}, \hat{f}_k) \tag{19c}$$
$$e_k = e_{k-1} + (v_{r,k} - v_k)T \tag{19d}$$
$$v_k = (p_k - p_{k-1})/T \tag{19e}$$
$$v_{d,k} = (p_{d,k} - p_{d,k-1})/T \tag{19f}$$

where T denotes the sampling interval of the controller and k is the index of the discrete time.

We can rewrite (19b) as follows by eliminating $v_{r,k}$ and e_k by combining it with (19a) and (19d):

$$\hat{f}_k \in \Gamma(v_{f,k} + \hat{f}_k/A, \mathrm{sgn}(v_{s,k} - v_{f,k} - \hat{f}_k/A)) \tag{20a}$$

where

$$v_{f,k} \triangleq v_k - (Ke_{k-1} - \hat{g}_k)/A \tag{20b}$$
$$v_{s,k} \triangleq (p_{d,k} + Hv_{d,k} - p_k)/H \tag{20c}$$
$$A \triangleq KT + B. \tag{20d}$$

It has been pointed out in [27] that the following relation holds true:

$$f \in \Gamma(v_b + \eta f, \mathrm{sgn}(v_a - \eta f)) \iff f = \mathrm{sat}_{\Gamma_s(\eta, v_b, \mathcal{B})}(v_a/\eta). \tag{21}$$

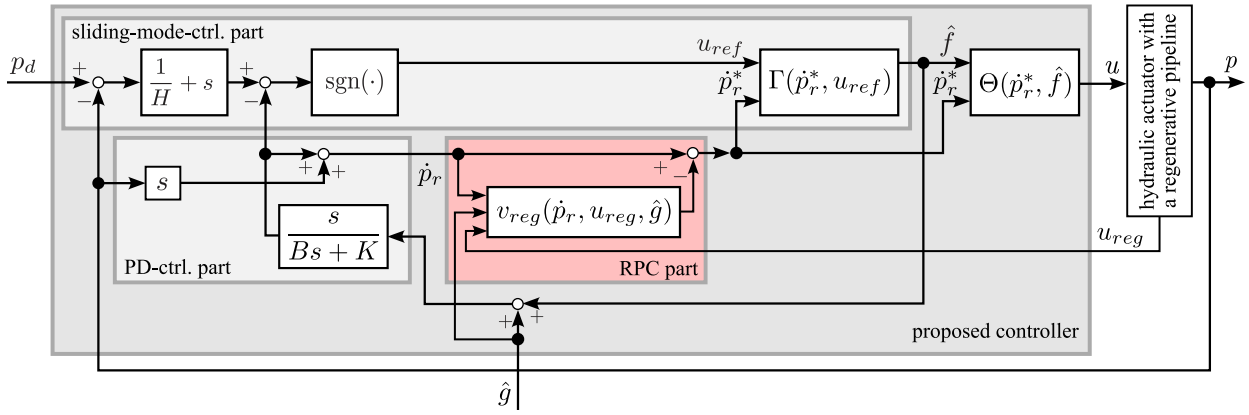

Fig. 5. Block diagram of the proposed controller with the regenerative-pipeline compensation (RPC). The opening ratio u_{reg} of the regenerative pipeline is determined by the built-in controller of the actuator and is assumed to be readable from the proposed controller. The set-valued functions Γ and Θ are determined according to the structure of the hydraulic circuit.

By using (19), (20), and (21), we can obtain an algorithm of the controller (15) to calculate u_k from the inputs $\{p_k, p_{d,k}, \hat{g}_k\}$ as follows:

$$v_k \coloneqq (p_k - p_{k-1})/T \tag{22a}$$
$$v_{d,k} \coloneqq (p_{d,k} - p_{d,k-1})/T \tag{22b}$$
$$v_{s,k} \coloneqq (p_{d,k} - p_k + Hv_{d,k})/H \tag{22c}$$
$$v_{f,k} \coloneqq v_k - (Ke_{k-1} - \hat{g}_k)/A \tag{22d}$$
$$\hat{f}_k \coloneqq \mathrm{sat}_{\Gamma_s(1/A, v_{f,k}, \mathcal{B})}(A(v_{s,k} - v_{f,k})) \tag{22e}$$
$$v_{r,k} \coloneqq v_{f,k} + \hat{f}_k/A \tag{22f}$$
$$e_k \coloneqq e_{k-1} + (v_{r,k} - v_k)T \tag{22g}$$
$$u_k \coloneqq \Theta_s(v_{r,k}, \hat{f}_k). \tag{22h}$$

Here, the single-valued function Θ_s is defined to satisfy (11) and its specific form is presented in [14].

D. Extension to Deal with Regenerative Pipeline

When the circuit includes a regenerative pipeline as in Fig. 2, the function Γ in the plant model does not match the quasistatic property of the actual plant, and thus the use of the functions Γ_s and Θ_s in the controller needs to be reconsidered. As discussed in Section II-C, the previous study [15] provided a version of Γ with the regenerative pipeline, but it is computationally costly and its correspondent Θ_s function is not yet available. Thus, we here present a controller with an approximated model.

Assuming that the ratio A_r/A_h is close to 1 and the pressure drop $F_r/A_r - F_h/A_h$ across the two chambers is caused by the external force g, we approximate (12), which represents quasistatic characteristics of an actuator with a regenerative pipeline, by the following form:

$$f \in \Gamma(\dot{p} - v_{reg}(\dot{p}, u_{reg}, g), u) \tag{23}$$

where

$$v_{reg}(v, u_{reg}, g) \triangleq \mathrm{sat}_{[0, 0.9v]}(c_{reg} u_{reg} \mathcal{R}(g/\bar{A}^3)), \tag{24}$$

$\bar{A} \triangleq (A_r + A_h)/2$, and g is the tensile external force applying to the actuator. The function v_{reg} involves a saturation, of which range is $[0, 0.9v]$, in order to satisfy the condition $0 < v_{reg}(v, u_{reg}, g) \leq v$, which is derived in [15].

One can see that the extended model (23) is the one in which v is replaced by $v - v_{reg}(\cdot)$ in the original use (7) of the function Γ. The same idea can be applied to the usages of the functions Θ, Γ_s, and Θ_s. Thus, the proposed controller (15) with the extension considering the regenerative pipelines can be obtained as follows:

$$\hat{f} = K(p_r - p) + B(\dot{p}_r - \dot{p}) - \hat{g} \tag{25a}$$
$$\hat{f} \in \Gamma(\dot{p}_r - v_{reg}(\dot{p}_r, u_{reg}, \hat{g}), \mathrm{sgn}(p_d - p + H(\dot{p}_d - \dot{p}_r))) \tag{25b}$$
$$u \in \Theta(\dot{p}_r - v_{reg}(\dot{p}_r, u_{reg}, \hat{g}), \hat{f}). \tag{25c}$$

Fig. 5 shows the overall structure of the controller (25). We here assume that u_{reg}, the valve opening ratio of the regenerative pipeline, is determined by the internal, built-in controller of the actuator, and thus cannot be manipulated by our controller. We however assume that, as shown in Fig. 5, u_{reg} is readable from our controller. We also assume that the estimated tensile external force $\hat{g}$ is available by some estimation methods, such as those based on the gravity calculated from the nominal masses of the links.

In a similar manner as we derived (22) from (15), one can obtain a discrete-time implementation of (25) as follows:

$$v_k \coloneqq (p_k - p_{k-1})/T \tag{26a}$$
$$v_{d,k} \coloneqq (p_{d,k} - p_{d,k-1})/T \tag{26b}$$
$$v_{k,reg} \coloneqq v_{reg}(v_{r,k-1}, u_{reg,k}, \hat{g}_k) \tag{26c}$$
$$v_{s,k} \coloneqq (p_{d,k} - p_k + Hv_{d,k})/H \tag{26d}$$
$$v_{f,k} \coloneqq v_k - (Ke_{k-1} - \hat{g}_k)/A \tag{26e}$$
$$\hat{f}_k \coloneqq \mathrm{sat}_{\Gamma_s(1/A, v_{f,k} - v_{k,reg}, \mathcal{B})}(A(v_{s,k} - v_{f,k})) \tag{26f}$$
$$v_{r,k} \coloneqq v_{f,k} + \hat{f}_k/A \tag{26g}$$
$$e_k \coloneqq e_{k-1} + (v_{r,k} - v_k)T \tag{26h}$$
$$u_k \coloneqq \Theta_s(v_{r,k} - v_{k,reg}, \hat{f}_k). \tag{26i}$$

Note that the only difference of the algorithm (26) from the algorithm (22) is the subtraction of $v_{k,reg}$ from $v_{f,k}$ in (26f) and (26i), and when $v_{k,reg}$ is set zero, (26) reduces to (22).

IV. SOME ANALYSES

A. Stability Analysis

This section shows a stability analysis of the proposed controller (15) applied to the plant (13). Recall that the controller (15) can be equivalently rewritten as (16). The closed-loop system composed of the plant (13) and the controller (16) can be written as follows:

$$\sigma = p - p_d + H(v - \dot{p}_d) \tag{27a}$$
$$\dot{e} = (\hat{f} + \hat{g} - Ke)/B \tag{27b}$$
$$\dot{v} = (f + g)/M \tag{27c}$$
$$v_r = v + \dot{e} \tag{27d}$$
$$f \in \Gamma(v, \Theta(v_r, \hat{f})) \tag{27e}$$
$$\hat{f} \in \Gamma(v_r, \mathrm{sgn}(-\sigma/H - \dot{e})). \tag{27f}$$

Here, we introduce the following functions $\tilde{\Gamma}$ and $\overline{\beta}$:

$$\tilde{\Gamma}(b, v_r, \hat{f}) \triangleq \Gamma(v_r - b, \Theta(v_r, \hat{f})) - \hat{f} \tag{28}$$

$$\overline{\beta}(b, v_r, \hat{f}) \triangleq \begin{cases} \dfrac{\tilde{\Gamma}(b, v_r, \hat{f})}{b} & \text{if } b \neq 0 \\ \min\left(\lim\limits_{b \to 0^+} \dfrac{\tilde{\Gamma}(b, v_r, \hat{f})}{b}, \lim\limits_{b \to 0^-} \dfrac{\tilde{\Gamma}(b, v_r, \hat{f})}{b} \right) & \text{otherwise.} \end{cases} \tag{29}$$

By employing the function (29) and the relation (21), we can rewrite the system (27) as follows:

$$\dot{\sigma} = v - \dot{p}_d + H(\dot{v} - \ddot{p}_d) \tag{30a}$$
$$\dot{e} = (\hat{f} + \hat{g} - Ke)/B \tag{30b}$$
$$\dot{v} = (\hat{f} + \beta\dot{e} + g)/M \tag{30c}$$
$$\hat{f} = \mathrm{sat}_{\Gamma_s(1/B, v - (Ke - \hat{g})/B, \mathcal{B})}(-B\sigma/H + Ke - \hat{g}) \tag{30d}$$

where

$$\beta = \overline{\beta}(\dot{e}, v + \dot{e}, \hat{f}). \tag{31}$$

At present, although it is not very conclusive, we have the following result in regard to properties of the closed-loop system (30):

Theorem 1: With the system (30), the state $[\sigma, v - \dot{p}_d, e]^T$ is uniformly ultimately bounded [28, Definition 4.6] if there exist $\delta > 0$ and $\alpha > 0$ with which

$$M < B\left(B + HK\right)/K \tag{32}$$
$$\delta\mathcal{B} \subset \Gamma_s(1/B, \dot{p}_d + \hat{g}/B, \mathcal{B}) + \hat{g} \tag{33}$$
$$|g - \hat{g} - M\ddot{p}_d| < \alpha \tag{34}$$

are satisfied, α is sufficiently small, and $|\dot{\beta}|$ is sufficiently small. In addition, if $g \equiv \hat{g}$ and $\ddot{p}_d \equiv 0$ are satisfied as well, the origin $[\sigma, v - \dot{p}_d, e]^T = 0$ is asymptotically stable.

The proof of Theorem 1 is provided in Appendix A. The requirement that $|\dot{\beta}|$ should be sufficiently small may or may not be restrictive and at least it hampers the completeness of the result. The incompleteness stems from the fact that the dynamics of β is not fully analyzed in the proof. It leaves the possibility that some particular patterns of temporal changes in β might make the state diverge. It however does not seem likely in practice considering that the term with β acts as a damping term that dissipates the energy. A more thorough proof considering the dynamics of β remains as an open problem to be addressed.

B. Parameter Tuning

This section provides some analyses that can be used for tuning the parameters $\{K, B, H\}$ of the controller (15). We employ another equivalent form (16) of the controller (15) for discussing the parameter tuning. Let us consider the case where the control input u is not saturated, i.e., the case where $-\sigma/H - \dot{e} = 0$ is satisfied. In this case, the intended actuator force $\hat{f}$ and the state variable $\dot{p}_r$ of the controller (16) are determined to satisfy both $-\sigma/H - \dot{e} = 0$ and (16a). Therefore, in this case, we can rewrite the controller (16) as follows:

$$\hat{f} = K_a(p_d - p) + B(v_d - v) + L_a \int (p_d - p)dt - \hat{g} \tag{35a}$$
$$v_r = v_d + (p_d - p)/H \tag{35b}$$
$$u \in \Theta(v_r, \hat{f}) \tag{35c}$$
$$\dot{p}_r = v_r, \quad \dot{p} = v, \quad \dot{p}_d = v_d \tag{35d}$$

where $K_a \triangleq K + B/H$ and $L_a \triangleq K/H$. The intended actuator force $\hat{f}$ is determined by the PID controller (35a). The state variable v_r is determined by the positional error $p_d - p$ and the target velocity $\dot{p}_d$.

We consider the closed-loop system composed of the controller (35) and the plant (13) with deadtime T_d because the hydraulic systems of commercial excavators are known to involve some deadtime [2], [4], [14]. The closed-loop system can be expressed as follows:

$$\hat{f} = K_a(p_d - p) + B(v_d - v) + L_a \int (p_d - p)dt - \hat{g} \tag{36a}$$
$$v_r = v_d + (p_d - p)/H \tag{36b}$$
$$f \in \Gamma(v(t + T_d), \Theta(v_r, \hat{f})) \tag{36c}$$
$$M\dot{v}(t + T_d) = f + g. \tag{36d}$$

Here, variables without arguments are functions of time t but the argument t is omitted for brevity.

Let us assume that, with $\{v_r, \hat{f}\}$ in (36c), $\Theta(v_r, \hat{f})$ is single-valued, and that $\Theta(v_r, \hat{f}) \in [-1, 1]$ and $\hat{f} \in [-F_{rM}, F_{hM}]$ hold true. Then, from the first-order Taylor expansion of $\Gamma(v, \Theta(v_r, \hat{f}))$ with respect to v around $v = v_r$, the following approximation holds:

$$\Gamma(v, \Theta(v_r, \hat{f})) \approx \hat{f} + \kappa(v_r, \hat{f})(v_r - v) + \mathcal{O}((v_r - v)^2) \tag{37}$$

where

$$\kappa(v_r, \hat{f}) \triangleq -\left.\frac{\partial \Gamma(v, u)}{\partial v}\right|_{v = v_r, u = \Theta(v_r, \hat{f})}. \tag{38}$$

Due to the properties of the function Γ discussed in [15], $\kappa(v_r, \hat{f}) \geq 0$ is always satisfied. Eliminating f and $\hat{f}$ from (36) by using the approximation (37) and assuming $\hat{g} = g$, we can rewrite the system (36) as following:

$$M\dot{v}(t + T_d) = K_a(p_d - p) + B(v_d - v) +$$

$$L_a \int (p_d - p)dt + \kappa(v_r, \hat{f})(v_r - v(t + T_d)). \tag{39}$$

Eq. (39) means that the controlled object is driven by a PID controller with an additional viscosity-like term. Assuming κ is constant, we can obtain the transfer function $G(s)$ of the system (39) as follows:

$$G(s) = \frac{\mathcal{L}[p]}{\mathcal{L}[p_d]} = \frac{(Hs+1)(s(\kappa+B)+K)}{HMe^{sT_d}s^3 + (\kappa e^{sT_d} + B)Hs^2 + (\kappa + B + HK)s + K} \tag{40}$$

where $\mathcal{L}$ represents the Laplace transform.

The pole locations of the transfer function $G(s)$ in (40) can be used for tuning the parameters $\{K, B, H\}$ because they represent the response characteristics of the system. In particular, for achieving smooth convergence without overshoots, the poles should be located on the real axis in the left-half plane. In order to obtain the poles, one needs to set an appropriate value to κ, which is the sign-reversed slope of the function Γ in the v direction. As has been detailed in previous papers [14], [27], the set-valued function Γ satisfies $\Gamma(0,0) = [-F_{hM}, F_{rM}]$ and it is monotone with respect to $-v$ (i.e., monotonically decreasing with respect to v). Therefore, to investigate the system behavior around the equilibrium $p_d = p \wedge v = 0$, a possible choice of κ can be given as follows:

$$\kappa \approx \frac{F_{rM} + F_{hM}}{\Delta v} \tag{41a}$$

where

$$\Delta v \triangleq \frac{\min(F_{rM}, F_{hM})T}{M}. \tag{41b}$$

Here, Δv can be seen as the maximum velocity that can be reached within the sampling interval T from $v = 0$, and thus $-\kappa$ can be seen as an effective slope value of $\Gamma(v, u)$ around $v = 0 \wedge u = 0$ in the discrete-time domain. Section V-B will present some numerical examples and simulation results supporting this approach.

V. Simulations

A. Setup

A realtime simulator of a 13-ton class hydraulic excavator was employed to validate the proposed controller. The simulator was constructed with Microsoft Visual C++ and the controller was constructed with MATLAB/Simulink. They were connected to each other through UDP/IP sockets at the cycle of 10 ms, i.e., the controller's sampling interval was $T = 10$ ms. The simulator's timestep size was 0.1 ms.

In the simulator, the links of the excavator, i.e., the boom, the arm, and the attachment as shown in Fig. 6, were treated as rigid bodies connected through virtual viscoelastic elements and virtual beams as illustrated in the green circle in Fig. 6. The stiffness and the viscosity of the virtual viscoelastic elements were 5.0×10^7 N/m and 3.0×10^5 N·s/m, respectively, and the length of the virtual beams was 2.0 m. The frictions in the joints were implemented by the technique presented in [29].

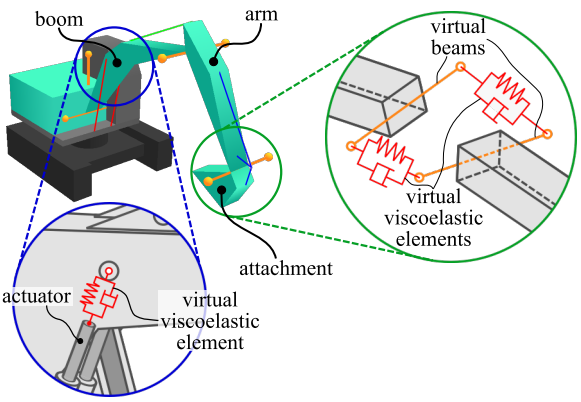

Fig. 6. Connections among links and actuators in the simulator, through virtual viscoelastic elements. The virtual viscoelastic elements emulate the compressibility of the oil in the actuators and the compliance of the links.

TABLE I
Parameters of the hydraulic actuators in the simulator.

symbols	physical meanings	boom	arm
P_{hM}	pressure limit of the head-side relief valves	35 MPa	35 MPa
P_{rM}	pressure limit of the rod-side relief valves	35 MPa	35 MPa
P_M	pressure limit of the pump relief valve	35 MPa	35 MPa
Q	oil flowrate from the pump	3.7×10^{-3} m^3/s	2.0×10^{-3} m^3/s
a_{ph}	MA[1] of MCV[2] connected to the pump and the head-side chamber	1.9×10^{-4} m^2	2.6×10^{-5} m^2
a_{pr}	MA[1] of MCV[2] connected to the pump and the rod-side chamber	1.7×10^{-5} m^2	1.5×10^{-4} m^2
a_{tr}	MA[1] of MCV[2] connected to the tank and the head-side chamber	6.5×10^{-5} m^2	6.2×10^{-5} m^2
a_{th}	MA[1] of MCV[2] connected to the tank and the rod-side chamber	7.2×10^{-5} m^2	1.5×10^{-4} m^2
a_b	MA[1] of the bleed valve	1.8×10^{-4} m^2	1.5×10^{-4} m^2
u_b	ratio of the bleed valve opening area	0.1	0.1
C_*	discharge coefficients ($* \in \{ph, pr, tr, th, b\}$)	0.7	0.7
ρ	mass density of the oil	850 kg/m^3	850 kg/m^3

[1] MA stands for the maximum opening area.
[2] MCV stands for a main control valve.

Each of actuators in the simulator was driven by a hydraulic circuit of the structure illustrated in Fig. 2. The circuit of the arm actuator included the regenerative pipeline, while those of the other three, the swing, the boom, and the attachment actuators, did not. The forces of the actuators were calculated based on the quasistatic actuator model [15]. Some parameters of the actuators are shown in Table I. The actuators were connected to the links through a virtual viscoelastic element with the stiffness 5.0×10^7 N/m and the viscosity 3.0×10^5 N·s/m as illustrated in the blue circle in Fig. 6, employing the technique presented in [30].

In order to emulate the deadtime and the lag in the responses

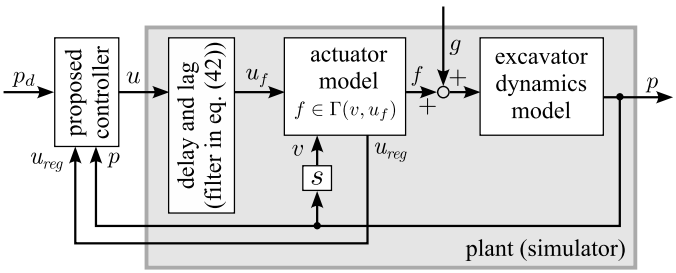

Fig. 7. Simulation setup. The actuator force f is calculated by the function Γ representing a quasistatic actuator model [15]. The opening ratio u_{reg} of the regenerative pipeline is determined by the built-in controller of the actuator and is used in the proposed controller, i.e., the algorithm (26).

of the main control valves of the actuators, the following filter was installed between the controller and the actuator as shown in Fig. 7:

$$u_f = \mathcal{L}^{-1}\left[\frac{\omega_0^2 e^{-T_d s}\mathcal{L}[u]}{s^2 + 2\zeta\omega_0 s + \omega_0^2}\right] \tag{42}$$

where T_d denotes the deadtime in the hydraulic system. The deadtime was set as $T_d = 0.3$ s. The filter (42) represents the combination of a second-order lag and the deadtime T_d in the response of the main control valves, where we set $\omega_0 = 94.2 (\approx 30\pi)$ rad/s and $\zeta = 1$.

As has been stated in Section III-D, the valve opening ratio u_{reg} of the regenerative pipeline of the arm actuator is assumed to be determined by a built-in controller and is assumed to be available to our position controller. In the simulations, to determine u_{reg}, we used a proprietary algorithm of the built-in controller provided by Kobelco Construction Machinery Co. Ltd., of which the details are not reported here.

B. Step Responses

We conducted some simulations to investigate the effect of the poles of the transfer function $G(s)$ in (40) in Section IV-B. In the simulations, step inputs of the target position p_d were provided to each of the boom and arm controllers with three different parameter settings. The gravitational forces calculated from the mass parameters of each link were employed as the external forces $\hat{g}$ of the boom and arm controllers. For the boom controller, the following settings were used:

- Setting $\mathrm{A_{bm}}$: $K = 2.5{\times}10^5$ N/m, $B = 2.5{\times}10^2$ N·s/m, $H = 0.5$ s.
- Setting $\mathrm{B_{bm}}$: $K = 2.5{\times}10^5$ N/m, $B = 2.5{\times}10^2$ N·s/m, $H = 1.0$ s.
- Setting $\mathrm{C_{bm}}$: $K = 5.0{\times}10^8$ N/m, $B = 2.5{\times}10^2$ N·s/m, $H = 1.0$ s.

For the arm controller, the following settings were used:

- Setting $\mathrm{A_{am}}$: $K = 1.5{\times}10^6$ N/m, $B = 2.0{\times}10^4$ N·s/m, $H = 0.5$ s.
- Setting $\mathrm{B_{am}}$: $K = 1.5{\times}10^6$ N/m, $B = 2.0{\times}10^4$ N·s/m, $H = 1.0$ s.
- Setting $\mathrm{C_{am}}$: $K = 1.5{\times}10^8$ N/m, $B = 2.0{\times}10^4$ N·s/m, $H = 1.0$ s.

The inertia M in the transfer function $G(s)$ in (40) were set as follows:

$$\hat{M}_* = \frac{I_*}{J_*(\theta_*)^2} \tag{43}$$

where $J_*(\theta_*) \triangleq \partial\Psi_*(\theta_*)/\partial\theta_*$ $(* \in \{\mathrm{bm}, \mathrm{am}\})$ and I_* are the total moments of inertia of the links around the actuator. The function Ψ_* is the kinematics from the joint angle θ_* to the actuator length p_*. The quantity $\hat{M}_*$ can be seen as an equivalent mass of the link seen from the actuator. We employed the equivalent masses $\hat{M}_*$ at the joint angles $\theta_{\mathrm{bm}} = 70°$ and $\theta_{\mathrm{am}} = 40°$, which were $\hat{M}_{\mathrm{bm}} = 2.5{\times}10^5$ kg and $\hat{M}_{\mathrm{am}} = 6.25{\times}10^4$ kg. We used $T_d = 0.3$ s for the transfer function $G(s)$ in (40) and used the first-order Padé approximation to approximate $G(s)$ by a rational function.

Figs. 8(a)(b)(c) show the relations among pole locations and step responses of the boom actuator. Fig. 8(a) shows the pole locations of the boom-actuator system with three parameter settings. Fig. 8(b) illustrates two motions of the step-response simulations, which are the boom-up and boom-down motions. Fig. 8(c) shows their results. From Fig. 8(c), one can see that Setting $\mathrm{B_{bm}}$ is the most suitable among the three settings because the actuator length p_b converged to the target length $p_{d,b}$ without overshoots or oscillations. The smooth and overdamped response of Setting $\mathrm{B_{bm}}$ in Fig. 8(c) is consistent with the green poles in Fig. 8(a) located on the real axis in the left-half plane. In contrast, Setting $\mathrm{A_{bm}}$ resulted in overshoots in Fig. 8(c), and it is consistent with the red poles in Fig. 8(a) in the left-half plane away from the real axis. With Setting $\mathrm{C_{bm}}$, the response became oscillatory though not divergent in Fig. 8(c), and the correspondent poles in Fig. 8(a) are unstable, in the right-half plane. The non-divergent results may be explained by the saturations of the control input $u \in [-1, 1]$ and the actuator force $f \in [-F_{rM}, F_{hM}]$.

Fig. 9(a)(b)(c) show the relations among pole locations and step responses of the arm actuator. Fig. 9(a) shows the pole locations of the arm-actuator system with three parameter settings. Fig. 9(b) illustrates two motions of the step-response simulations, which are the arm-up and arm-down motions. Fig. 9(c) shows their results. It shows that Setting $\mathrm{B_{am}}$ resulted in the most favorable behaviors in both arm-up and arm-down motions. These results are consistent with the locations of the green poles in Fig. 9(a), as has been the case with the results with boom motions. One can see that Setting $\mathrm{B_{am}}$ produced small fluctuation in p_{am} in $t \in [1\text{ s}, 2\text{ s}]$ of the arm-down motion, which can be attributed to the inaccuracy of the compensation of the regenerative pipeline's effect. The responses with Setting $\mathrm{A_{am}}$ in Fig. 9(c) results in overshoots, which are consistent with the red poles away from the real axis shown in Fig. 9(a). As has also been the case with the boom results, from Fig. 9(c), Setting $\mathrm{C_{am}}$ resulted in oscillatory responses, although its blue poles in Fig. 9(a) are unstable. It can be attributed to the saturations of u and f.

C. Effects of Errors in the Actuator Models

Some simulations were conducted to test the influence of parametric errors in the actuator models. The modeling errors

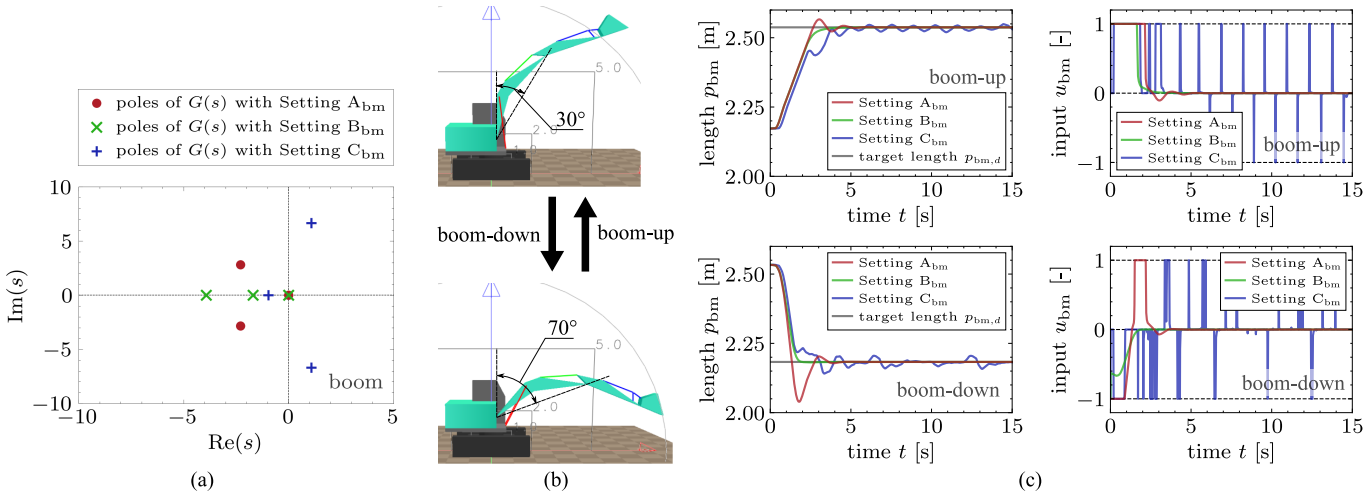

Fig. 8. Simulation of step responses of the boom actuator with three different parameter settings, which are Settings A_{bm}, B_{bm}, and C_{bm} shown in Section V-B. (a) Poles of the transfer function $G(s)$ in (40). (b) Configuration of the excavator. (c) Step responses of the boom.

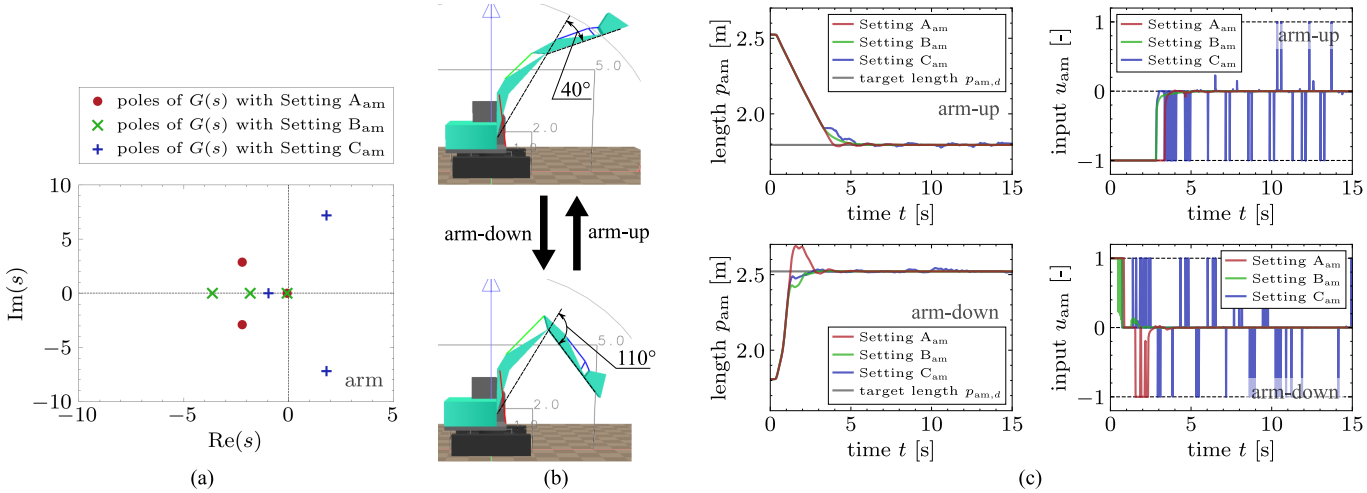

Fig. 9. Simulation of step responses of the arm actuator with three different parameter settings, which are Settings A_{am}, B_{am}, and C_{am} shown in Section V-B. (a) Poles of the transfer function $G(s)$ in (40). (b) Configuration of the excavator. (c) Step responses of the arm.

were generated by randomly varying all actuator parameters including those in Table I by -10 %, 0, or $+10$ %, and the number of trials for each controller was 100. We tested three controllers, which were the proposed controller with the regenerative-pipeline compensation, that without the regenerative-pipeline compensation, and the following PID controller:

$$\hat{f} = K_a(p_d - p) + B(\dot{p}_d - \dot{p}) + L_a \int (p_d - p)dt - \hat{g} \quad (44a)$$

$$v_r = \dot{p}_d + (p_d - p)/H \quad (44b)$$

$$u = \Theta_s(v_r, \hat{f}) \quad (44c)$$

where $K_a \triangleq K + B/H$ and $L_a \triangleq K/H$. Note that, as has been shown in Section IV-B, the PID controller (44) is equivalent to the proposed controller (15) when u and $\hat{f}$ are unsaturated.

The simulations were performed as illustrated in Fig. 10(a), in which the target position $\boldsymbol{r}_d$ was moved along a square trajectory. The velocity $\|\dot{\boldsymbol{r}}_d\|$ was set triangular as shown in Fig. 10(b). The controllers were implemented to each of the boom and the arm actuators, and the target length $\{p_{bm,d}, p_{am,d}\}$ of the actuators were computed through the inverse kinematics from the target arm-tip position $\boldsymbol{r}_d$. The controller parameters were chosen as the same as Settings B_{bm} and B_{am}, which provided favorable pole placements and step-response results in Section V-B.

Figs. 11(a) and (b) show results with the proposed controller with and without the regenerative-pipeline compensation, respectively. In all cases, the position $\boldsymbol{r}$ converged to the target position $\boldsymbol{r}_d$. From the comparison between the almost ideal case (the red line) in Fig. 11(a) and that in Fig. 11(b), one can see that the regenerative-pipeline compensation reduces the positional errors. The chattering-like behavior of the control input u_{am} in Fig. 11(b) may be because the total modeling errors may have been too large for the controller without compensation for the regenerative pipeline.

Fig. 11(c) shows simulation results with the PID controller (44). The comparison between Fig. 11(b) and Fig. 11(c) suggests that the proposed controller, even without the

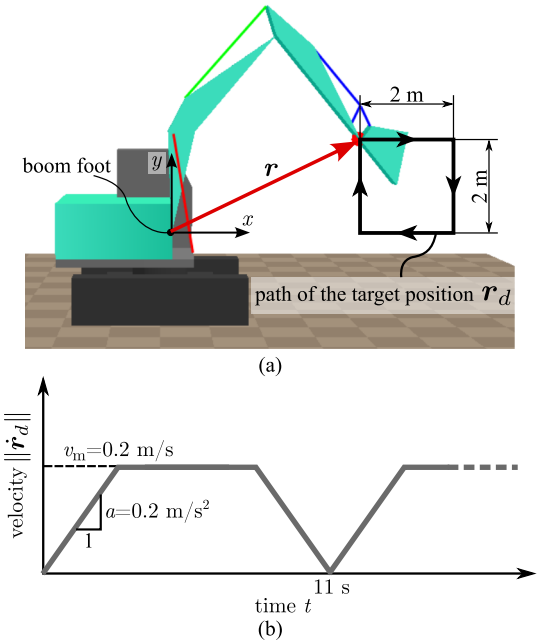

Fig. 10. Target trajectory $\boldsymbol{r}_d(t)$; (a) the trajectory of $\boldsymbol{r}_d(t)$ and the coordinate system, (b) the target velocity $\|\dot{\boldsymbol{r}}_d\|$, which is triangular.

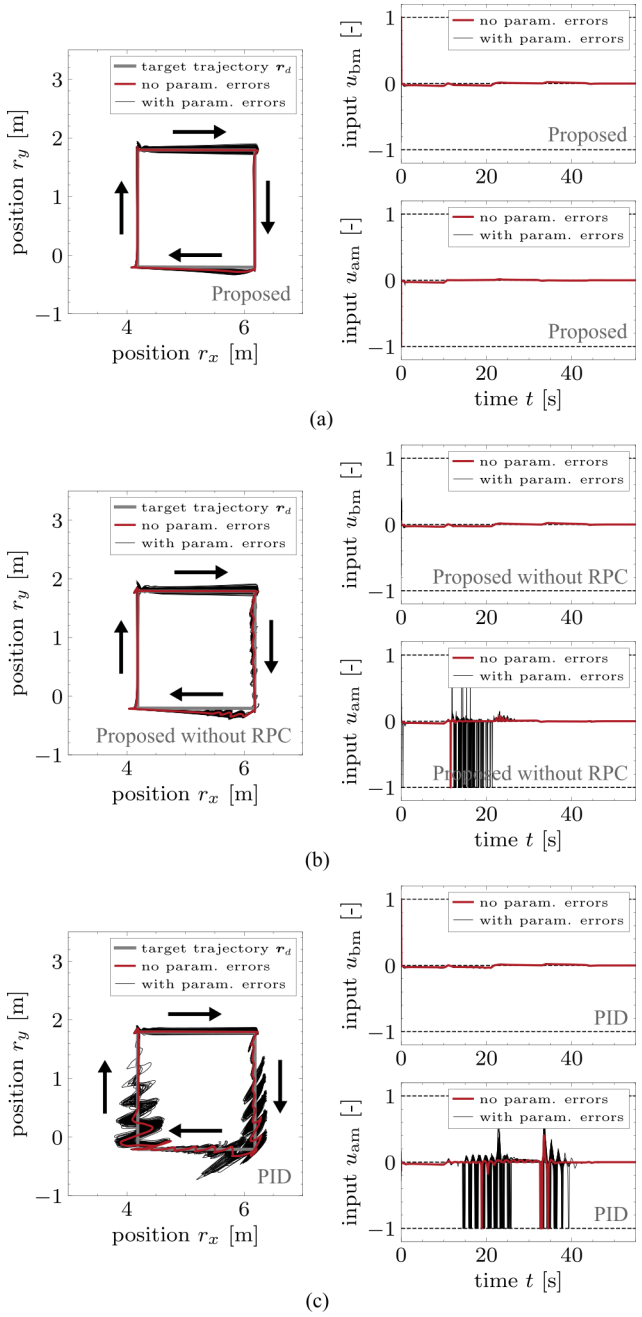

Fig. 11. Simulation results with modeling errors that were randomly selected in $\{-10\,\%, 0, +10\,\%\}$ for parameters of the actuators. The red lines show an almost ideal case with no modeling errors. The number of trials was 100 for each configuration. The deadtime T_d was set as 300 ms. (a) The proposed controller. (b) The proposed controller without the regenerative-pipeline compensation (RPC). (c) PID controller (44).

regenerative-pipeline compensation, resulted in higher accuracy and smaller oscillations than the PID controller (44). Recalling that (44) is equivalent to the proposed controller (15) as long as $\hat{f}$ and u are unsaturated and considering that the regenerative pipeline acts as a modeling error, one can see that the sliding-mode structure of the proposed controller, which is intended to handle the saturation, contributes to higher robustness against modeling errors.

VI. Experiments

A. Setup

We tested the proposed controller with a 13-ton class excavator, Kobelco SK135SRD-5 with a shear-type attachment, shown in Fig. 12. The excavator had three links as shown in Fig. 12, which were the boom, the arm, and the attachment. Each of the actuators was driven by a hydraulic circuit of the structure illustrated in Fig. 2, with a single four-port spool valve acting as the collection of the four main control valves in Fig. 2. The control input u from the controller was interpreted as the spool position of the spool valve. The arm actuator involved the regenerative pipeline, while the boom actuator did not. The hydraulic circuits of the boom and arm actuators were interconnected through some pipelines, but during the experiments, the interconnecting pipelines were hardly in effect. Therefore, we regarded the circuits of the two actuators as independent from each other, each of them being driven by its own pump. Further detailed specifications and structures of the actuators are not provided in this paper due to proprietary restrictions.

The proposed controller was implemented to each of the boom and the arm actuators. The controller was constructed with MATLAB/Simulink and its sampling interval was set as $T = 0.01$ s. The controller was connected to the excavator over the Control Area Network (CAN). It commanded the opening ratios of the main control valves as the control input u through CAN and received the joint angles measured by potentiometers. The measured angles were converted into the actuator length p, which were used as the inputs to the controller. The parameters of the proposed controller for the boom actuator were set as $K = 2.5\times10^5$ N/m, $B = 2.5\times10^2$ N·s/m, and $H = 0.5$ s, which are the same as Setting $\mathrm{A_{bm}}$ shown

Fig. 12. Kobelco 13-ton class excavator with a shear attachment.

in Section V-B. The parameters for the arm actuator were set as $K = 1.5{\times}10^6$ N/m, $B = 2.0{\times}10^4$ N·s/m, and $H = 1.0$ s, which are the same as Setting $\mathrm{B_{am}}$. Although the parameters were chosen based on the discussion in Section IV-B, we additionally tuned them in the experiments. As a result, the parameter values for the boom were chosen to be different from those that were most suited in the simulations in Section V-B.

The valve opening ratio u_{reg} of the regenerative pipeline of the arm actuator was manipulated by a built-in controller of the excavator, and its algorithm is proprietary. The proposed controller implemented to the arm actuator uses the value of u_{reg} as an input.

In the experiments, we did not test other controllers including the PID controller (44). As a practical matter, we needed to avoid risky trials with the 13-ton class excavator using controllers that have not been adequately validated in our environment.

B. Step Responses

Some experiments were performed to check the step responses with the proposed controller. In the experiments, the excavator was moved as illustrated in Fig. 13(a) to examine the step responses of the boom actuator, and also as in Fig. 14(a) for the arm actuator.

Fig. 13(b) shows the results of the boom actuator. As seen in the figure, the length p_{bm} of the boom actuator smoothly converged to the target length $p_{\mathrm{bm},d}$ in both boom-up and boom-down motions. Fig. 13(b) also shows that the control input u_{bm} was saturated for the first few seconds, but it did not result in overshoots or oscillations after that. These results illustrate the effect of the sliding-mode structure of the proposed controller.

It should be noted that the employed parameter setting was not the same as the most suitable setting in the simulations in Section V-B, but resulted in no overshoots or oscillations in these experiments. The difference between the simulation and experiment results may be attributed to unmodeled factors of the excavator, such as joint frictions, the viscosity of the oil, and the compressibility of the oil.

Fig. 14(b) shows the results of the arm actuator. It shows similar features as those in Fig. 13(b), indicating that the controller properly worked also with the arm actuator. It shows some chattering-like behaviors in the control input u_{am}. It may be attributed to the imperfection of the regenerative-pipeline compensation, which can make the first argument of Θ_s in (26i) too small due to possible modeling errors. Such chattering in u_{am} would not be a practical issue because it does not result in physical vibration due to the dynamics of the spool valve and because it does not affect the convergence of the length p_{am}. Nevertheless, for improving the regenerative-pipeline compensation, it may be reasonable to employ a more accurate estimate of the external force $\hat{g}$ in (25c), e.g., an estimated force based on the chamber pressures.

In the experiments with the arm actuator, we employed Setting $\mathrm{B_{am}}$, which is the most suitable setting in the simulations in Section V-B. The experimental results were overall close to the simulation results with the same Setting $\mathrm{B_{am}}$ in Fig. 9(c), although there are more intense chattering-like behaviors in the control input u_{am} than the simulations.

The deadtime in the excavator was not accurately available, but it was estimated from the experimental results. From the zoomed graphs in Figs. 13(b) and 14(b), one can see that the time spent from the step input to the beginning of the motion was about 0.25 s and 0.15 s with the boom actuator, and 0.6 s and 0.35 s with the arm actuator, which can be seen as rough estimates of the deadtime. It should be noted that the proposed controller does not explicitly depend on the estimated deadtime, except that it may be used for the parameter tuning scheme discussed in Section IV-B. It should also be recalled that the controller parameters in the experiments were chosen by using the pole locations of the transfer function $G(s)$ in (40) with the estimated deadtime $T_d = 0.3$ s.

C. Trajectory-Tracking Control

We tested the proposed controller (15) with two trajectory-tracking tasks. The controller was implemented in each of the boom and arm actuators so that the arm-tip position $\boldsymbol{r}$ should follow the target position $\boldsymbol{r}_d$. The target lengths $\{p_{\mathrm{bm},d}, p_{\mathrm{am},d}\}$ of the actuators were computed from the target arm-tip position $\boldsymbol{r}_d$ through the inverse kinematics. The parameters were set the same as in the case of the step-response experiments in Section VI-B.

The first task was the tracking along a sloping-down trajectory shown in Fig. 15(a) with the trapezoidal pattern of the speed $\|\dot{\boldsymbol{r}}_d\|$ shown in Fig. 15(b). The results in Fig. 15(c) show that the tracking was properly achieved without oscillations or overshoots. Recall that the hydraulic actuators have a deadtime ranging from approximately 0.15 s to 0.6 s, as observed in the step responses shown in Figs. 13 and 14. For such actuators, the proposed controller, which does not explicitly compensate for the deadtime, achieved small positional errors and smooth convergence.

The second task was the tracking along a square-shaped trajectory shown in Fig. 16(a) with the trapezoidal speed pattern shown in Fig. 16(b). From the results in Fig. 16(c),

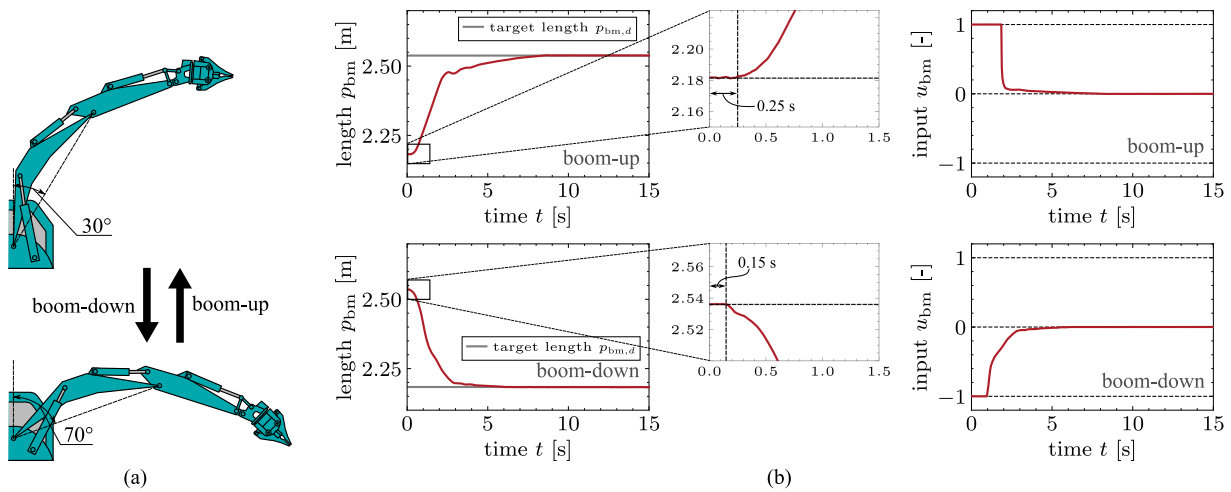

Fig. 13. Experiments of step responses of the boom actuators; (a) Configuration of the excavator and (b) step responses of the boom.

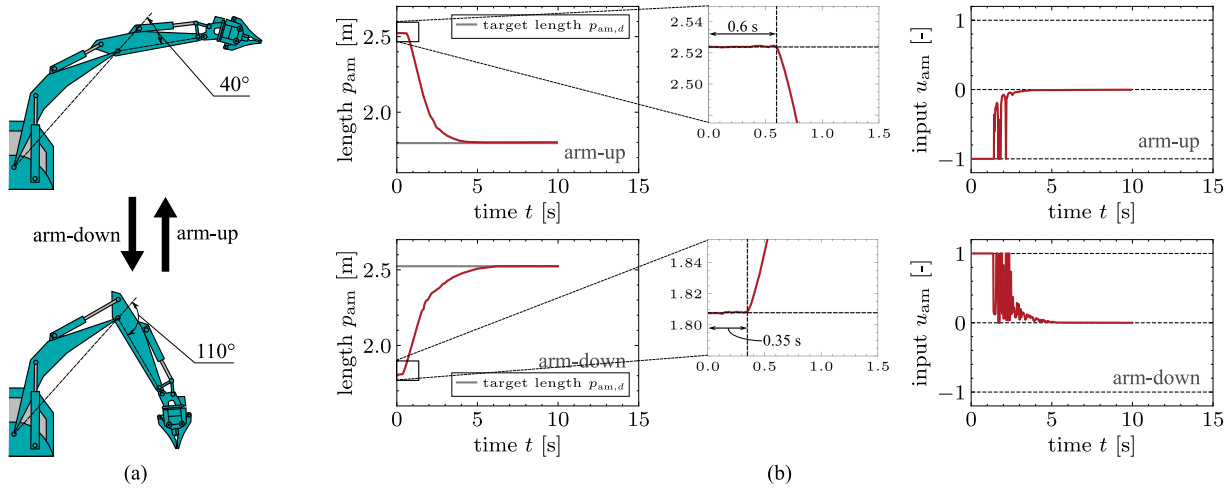

Fig. 14. Experiments of step responses of the arm actuators; (a) Configuration of the excavator and (b) step responses of the arm.

one can see that the tracking was mostly successful with the excavator, which has the deadtime and the regenerative circuit. There were, however, some oscillations during the motions along the top and right edges ($t \in [0\ \mathrm{s}, 18\ \mathrm{s}]$) of the trajectory, which coincided with the boom-down motion. The oscillations are visible in the graphs of the position $\boldsymbol{r}$, although it is not very visible in the graphs of the actuator lengths $\{p_{\mathrm{bm}}, p_{\mathrm{am}}\}$. The oscillations can be seen as a stick-slip-like phenomenon, which is presumably caused by the dead zone in the control valves and the joint friction. In fact, a careful examination of Fig. 16(c) revealed that the length p_{bm} started to move only when the control input u_{bm} was below -0.1. In addition, there were also some positional errors about 0.1 m during the motions along the bottom and left edges ($t \in [18\ \mathrm{s}, 26\ \mathrm{s}]$) of the trajectory. It may be attributed to the inaccuracy of the actuator model in the controller.

The oscillation and positional error may be suppressed by improving the actuator model in the controller, e.g., by including the dead zone of the control valves. In addition, the oil flowrate from the pump, which was treated as a constant in the present controller, may need to be substituted by measured values from an appropriate sensor.

VII. Conclusion

This paper has proposed a position controller for hydraulic actuators with deadtime and regenerative pipelines. The controller is constructed by combining a sliding-mode controller and a PD controller in a differential-algebraic manner, and incorporates a previously-proposed quasistatic model of hydraulic actuators. By employing the actuator model, the proposed controller accounts for the saturations of the actuator force. In addition, due to the use of the PD controller, it realizes a certain level of robustness against the presence of the deadtime. Furthermore, the controller has been extended to deal with regenerative pipelines in the hydraulic actuators. We also have provided some analyses that can be used for tuning the controller parameters. The proposed controller has been validated with simulations and experiments employing a 13-ton class excavator, which has deadtime of 0.1 s to 0.6 s and a regenerative pipeline in the arm actuator. In the simulations and experiments, it has been shown that some different tasks, including set-point control tasks and trajectory-

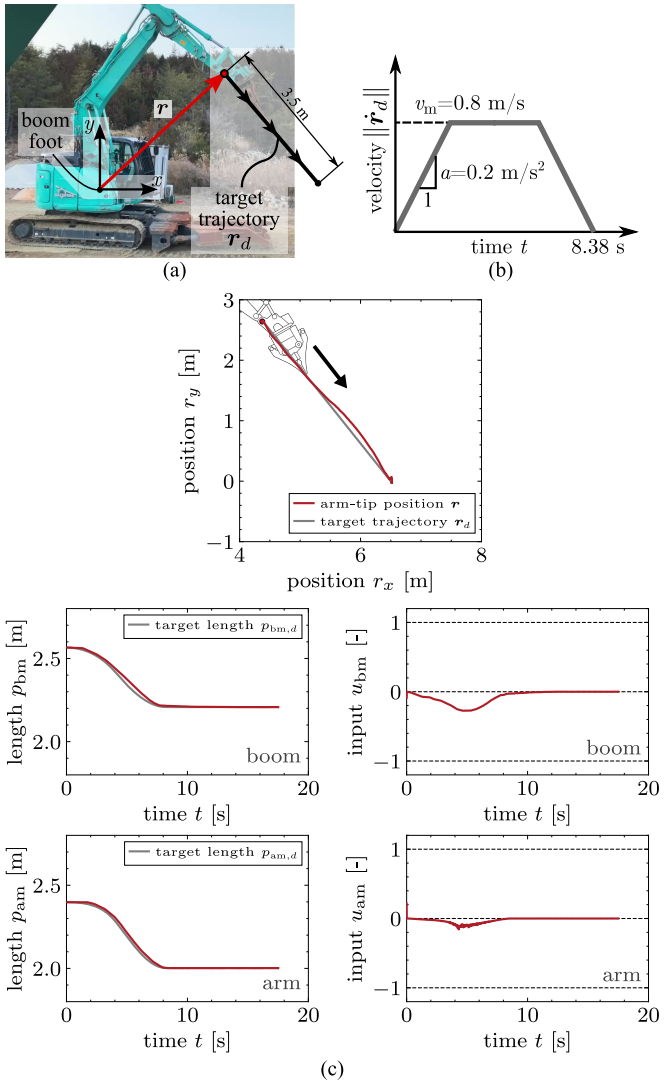

Fig. 15. Experiments of tracking along an oblique downward trajectory; (a) Target trajectory. (b) Velocity pattern. (c) Experimental results.

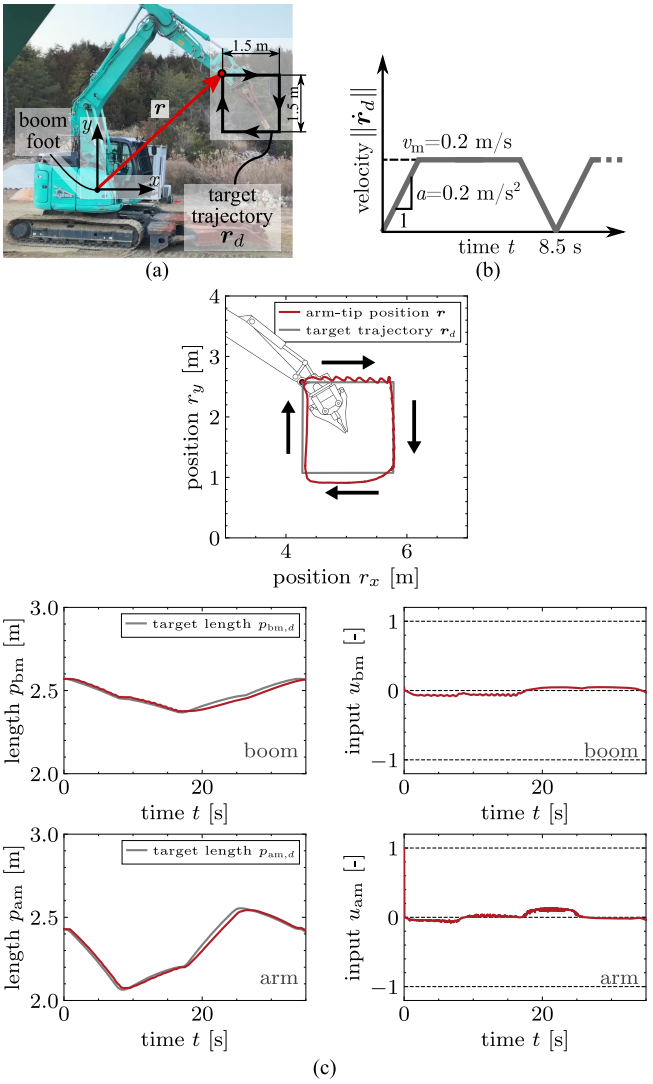

Fig. 16. Experiments of tracking along a square trajectory; (a) Target trajectory. (b) Velocity pattern. (c) Experimental results.

tracking tasks, can be achieved with a single common set of parameter settings.

Future work should address combining the controller with disturbance compensation techniques, probably based on the sensor information of the pressures and flowrates in the actuators and the circuits. It would enhance the accuracy of the controller, especially when the excavator is loaded. In addition, one should also consider the fact that, in commercial excavators, the structures of hydraulic circuits may be more involved than that has been considered in this paper; for example, a single pump may drive multiple actuators. The extension of the controller to deal with such complicated circuit structures should also be sought.

Appendix A
Proof of Theorem 1

Proof of Theorem 1: Let us define $v_e \triangleq v - \dot{p}_d$ and $\phi \triangleq g - \hat{g} - M\ddot{p}_d$. Then, the system (30) can be rewritten as follows:

$$\dot{\boldsymbol{x}} = \boldsymbol{A}(\beta)\boldsymbol{x} - \boldsymbol{b}(\beta)\,\mathrm{dzn}_{\Gamma_s(1/B,\boldsymbol{g}^T\boldsymbol{x}+\hat{g}/B+\dot{p}_d,\mathcal{B})}(\boldsymbol{c}^T\boldsymbol{x} - \hat{g}) + \boldsymbol{d}\phi \quad (45)$$

where

$$\boldsymbol{x} \triangleq [\sigma, v_e, e]^T \quad (46)$$

$$\boldsymbol{A}(\beta) \triangleq \begin{bmatrix} -(B+\beta)/M & 1 & HK/M \\ -(B+\beta)/(HM) & 0 & K/M \\ -1/H & 0 & 0 \end{bmatrix} \quad (47)$$

$$\boldsymbol{d} \triangleq [H/M, 1/M, 0]^T \quad (48)$$

$$\boldsymbol{b}(\beta) \triangleq [H(B+\beta)/(BM), (B+\beta)/(BM), 1/B]^T \quad (49)$$

$$\boldsymbol{c} \triangleq [-B/H, 0, K]^T \quad (50)$$

$$\boldsymbol{g} \triangleq [0, 1, -K/B]^T \quad (51)$$

$$\mathrm{dzn}_{\mathcal{X}}(f) \triangleq f - \mathrm{sat}_{\mathcal{X}}(f). \quad (52)$$

Here, we can use the following property of the function dzn

$$\mathrm{dzn}_{\mathcal{X}}(x-a) = \mathrm{dzn}_{\mathcal{X}+a}(x). \quad (53)$$

Then, we can rewrite (45) as follows:

$$\dot{\boldsymbol{x}} = \boldsymbol{A}(\beta)\boldsymbol{x} - \boldsymbol{b}(\beta)\,\mathrm{dzn}_{\mathcal{F}(\boldsymbol{g}^T\boldsymbol{x},\mathcal{B})}(\boldsymbol{c}^T\boldsymbol{x}) + \boldsymbol{d}\phi \tag{54}$$

where

$$\mathcal{F}(v,u) \triangleq \Gamma_s(1/B, v + \dot{p}_d + \hat{g}/B, u) + \hat{g}. \tag{55}$$

It can be shown that $\boldsymbol{A}(\beta)$ is Hurwitz for all $\beta \geq 0$ if (32) is satisfied. Therefore, for any diagonal and positive definite matrix $\boldsymbol{Q} \succ 0$, there exists a symmetric and positive definite matrix $\boldsymbol{P}(\beta) \succ 0$ with which

$$\boldsymbol{Q} = -(\boldsymbol{P}(\beta)\boldsymbol{A}(\beta) + \boldsymbol{A}(\beta)^T\boldsymbol{P}(\beta))/2 \tag{56}$$

is satisfied. With such a matrix $\boldsymbol{P}(\beta)$, let us define $V \triangleq \boldsymbol{x}^T\boldsymbol{P}(\beta)\boldsymbol{x}/2$. Then, we have

$$\begin{aligned}\dot{V} &= -\boldsymbol{x}^T\boldsymbol{Q}\boldsymbol{x} - \boldsymbol{x}^T\boldsymbol{P}(\beta)\boldsymbol{b}(\beta)\,\mathrm{dzn}_{\mathcal{F}(\boldsymbol{g}^T\boldsymbol{x},\mathcal{B})}(\boldsymbol{c}^T\boldsymbol{x}) + \\ &\quad \boldsymbol{x}^T\boldsymbol{P}(\beta)\boldsymbol{d}\phi + \boldsymbol{x}^T\boldsymbol{R}(\beta)\boldsymbol{x}\dot{\beta} \\ &\leq -(\lambda_Q - \gamma_R(\beta)|\dot{\beta}|)\|\boldsymbol{x}\|^2 + \alpha\|\boldsymbol{P}(\beta)\boldsymbol{d}\|\|\boldsymbol{x}\| + \\ &\quad \|\boldsymbol{P}(\beta)\boldsymbol{b}(\beta)\|\|\boldsymbol{x}\|\,|\,\mathrm{dzn}_{\mathcal{F}(\boldsymbol{g}^T\boldsymbol{x},\mathcal{B})}(\boldsymbol{c}^T\boldsymbol{x})|\end{aligned} \tag{57}$$

where

$$\boldsymbol{R}(\beta) \triangleq \frac{1}{2}\frac{\partial \boldsymbol{P}(\beta)}{\partial \beta}. \tag{58}$$

Here, λ_Q is the minimum eigenvalue of $\boldsymbol{Q}$ and $\gamma_R(\beta)$ is the maximum absolute value of the eigenvalues of $\boldsymbol{R}(\beta)$.

The matrix $\boldsymbol{P}(\beta)$ can be analytically obtained (by using, e.g., LyapunovSolve function of Mathematica) as a rational function of β. From the analytical representation of $\boldsymbol{P}(\beta)$, it can be seen that $\|\boldsymbol{P}(\beta)\boldsymbol{b}(\beta)\|$ and $\|\boldsymbol{P}(\beta)\boldsymbol{d}\|$ are bounded if (32) is satisfied. It can also be seen that all the elements of $\boldsymbol{R}(\beta)$ are bounded, and thus $\gamma_R(\beta)$ is also bounded.

Now, let us focus on the third term of the right-hand side of (57). With some straightforward derivations, the following can be seen:

$$\begin{aligned}|\,\mathrm{dzn}_{\mathcal{F}(v,\mathcal{B})}(f)| &= \max(0, f - \mathcal{F}(v,1)) + \\ &\quad \max(0, -f + \mathcal{F}(v,-1)).\end{aligned} \tag{59}$$

From the property of Γ_s, one can see that

$$-B \leq \frac{\partial \mathcal{F}(v,u)}{\partial v} \leq 0, \tag{60}$$

and thus the following is satisfied:

$$0 \leq v(\mathcal{F}(0,u) - \mathcal{F}(v,u)) \leq Bv^2. \tag{61}$$

It is equivalent to

$$\mathcal{F}(0,u) - B\max(v,0) \leq \mathcal{F}(v,u) \leq \mathcal{F}(0,u) - B\min(v,0), \tag{62}$$

which implies the following:

$$\mathcal{F}(0,u) - B|v| \leq \mathcal{F}(v,u) \leq \mathcal{F}(0,u) + B|v|. \tag{63}$$

By using (63), one can see that the terms of the right-hand side of (59) are upperbounded as follows:

$$\begin{aligned}\max(0, f - \mathcal{F}(v,1)) &\leq \max(0, f - \mathcal{F}(0,1) + B|v|) \\ &\leq \max(0, |f| + B|v| - \delta) \\ \max(0, -f + \mathcal{F}(v,-1)) &\leq \max(0, -f + \mathcal{F}(0,-1) + B|v|) \\ &\leq \max(0, |f| + B|v| - \delta).\end{aligned} \tag{64}$$

Here, we used the fact that $\mathcal{F}(0,-1) \leq -\delta$ and $\delta \leq \mathcal{F}(0,1)$ derived from the condition (33). Noting that the two terms of the right-hand side of (59) cannot be non-zero simultaneously, we have the following:

$$|\,\mathrm{dzn}_{\mathcal{F}(v,\mathcal{B})}(f)| \leq \max(0, |f| + B|v| - \delta). \tag{66}$$

By using (66) in (57), an upperboudnd of $\dot{V}$ can be given as follows:

$$\begin{aligned}\dot{V} &\leq -(\lambda_Q - \gamma_R(\beta)|\dot{\beta}|)\|\boldsymbol{x}\|^2 + \alpha\|\boldsymbol{P}(\beta)\boldsymbol{d}\|\|\boldsymbol{x}\| \\ &\quad \|\boldsymbol{P}(\beta)\boldsymbol{b}(\beta)\|\|\boldsymbol{x}\|\max(0, \|\boldsymbol{c}\|\|\boldsymbol{x}\| + B\|\boldsymbol{g}\|\|\boldsymbol{x}\| - \delta) \\ &\leq -c_0\|\boldsymbol{x}\|(\min(\|\boldsymbol{x}\|, -c_1\|\boldsymbol{x}\| + c_2) - \alpha c_3)\end{aligned} \tag{67}$$

where

$$c_0 \triangleq \lambda_Q - \overline{\gamma_R(\beta)}|\dot{\beta}| \tag{68}$$

$$c_1 \triangleq \overline{\|\boldsymbol{P}(\beta)\boldsymbol{b}(\beta)\|}(\|\boldsymbol{c}\| + B\|\boldsymbol{g}\|)/c_0 - 1 \tag{69}$$

$$c_2 \triangleq \delta\overline{\|\boldsymbol{P}(\beta)\boldsymbol{b}(\beta)\|}/c_0 \tag{70}$$

$$c_3 \triangleq \overline{\|\boldsymbol{P}(\beta)\boldsymbol{d}\|}/c_0. \tag{71}$$

Here, $\overline{\gamma_R(\beta)}$, $\overline{\|\boldsymbol{P}(\beta)\boldsymbol{b}(\beta)\|}$, and $\overline{\|\boldsymbol{P}(\beta)\boldsymbol{d}\|}$ are upperbounds of $\gamma_R(\beta)$, $\|\boldsymbol{P}(\beta)\boldsymbol{b}(\beta)\|$. and $\|\boldsymbol{P}(\beta)\boldsymbol{d}\|$, respectively. Therefore, $\dot{V} < 0$ is satisfied when $c_0 > 0$ and

$$\min(\|\boldsymbol{x}\|, -c_1\|\boldsymbol{x}\| + c_2) > \alpha c_3 \tag{72}$$

are satisfied. Here, (72) is equivalent to

$$\alpha c_3 < \|\boldsymbol{x}\| < \begin{cases}(c_2 - \alpha c_3)/c_1 & \text{if } c_1 > 0 \\ \infty & \text{otherwise.}\end{cases} \tag{73}$$

For the existence of $\boldsymbol{x}$ satisfying (73), when $c_1 > 0$, α must satisfy the following:

$$\alpha < \frac{c_2}{c_3(c_1+1)} = \frac{\delta(\lambda_Q - \overline{\gamma_R(\beta)}|\dot{\beta}|)}{\overline{\|\boldsymbol{P}(\beta)\boldsymbol{d}\|}(\|\boldsymbol{c}\| + B\|\boldsymbol{g}\|)}. \tag{74}$$

Therefore, if $|\dot{\beta}|$ is small enough to satisfy $|\dot{\beta}| < \lambda_Q/\overline{\gamma_R(\beta)}$ and if α is small enough to satisfy (74), one can say that the state $\boldsymbol{x}$ is uniformly ultimately bounded with the ultimate bound $\alpha c_3\mathcal{B}$, which is a neighborhood of the origin.

In addition, if $\alpha = 0$, i.e., if $\phi \equiv 0$ and $\ddot{p}_d \equiv 0$, $\dot{V} < 0$ is satisfied in $\boldsymbol{x} \in (c_2/c_1)\mathcal{B}$ if $c_1 < 0$ and globally otherwise. This means that the origin is asymptotically stable if $\phi \equiv 0$ and $\ddot{p}_d \equiv 0$.

REFERENCES

[1] J. Kim, M. Jin, W. Choi, and J. Lee, "Discrete time delay control for hydraulic excavator motion control with terminal sliding mode control," *Mechatronics*, vol. 60, pp. 15–25, 2019. doi: 10.1016/j.mechatronics.2019.04.008

[2] P. H. Chang and S.-J. Lee, "A straight-line motion tracking control of hydraulic excavator system," *Mechatronics*, vol. 12, no. 1, pp. 119–138, 2002. doi: 10.1016/S0957-4158(01)00014-9

[3] Y. Wang, L. Gu, B. Chen, and H. Wu, "A new discrete time delay control of hydraulic manipulators," *Proceedings of the Institution of Mechanical Engineers, Part I: Journal of Systems and Control Engineering*, vol. 231, no. 3, pp. 168–177, 2017. doi: 10.1177/0959651816689340

[4] S. Kim, J. Park, S. Kang, P. Y. Kim, and H. J. Kim, "A robust control approach for hydraulic excavators using μ-synthesis," *International Journal of Control, Automation and Systems*, vol. 16, no. 4, pp. 1615–1628, 2018. doi: 10.1007/s12555-017-0071-9

[5] Y. Ye, C.-B. Yin, Y. Gong, and J.-J. Zhou, "Position control of nonlinear hydraulic system using an improved PSO based PID controller," *Mechanical Systems and Signal Processing*, vol. 83, pp. 241–259, 2017. doi: 10.1016/j.ymssp.2016.06.010

[6] H. Feng, W. Ma, C. Yin, and D. Cao, "Trajectory control of electro-hydraulic position servo system using improved PSO-PID controller," *Automation in Construction*, vol. 127, p. 103722, 2021. doi: 10.1016/j.autcon.2021.103722

[7] H. Feng, C.-B. Yin, W.-W. Weng, W. Ma, J.-J. Zhou, W.-H. Jia, and Z.-L. Zhang, "Robotic excavator trajectory control using an improved GA based PID controller," *Mechanical Systems and Signal Processing*, vol. 105, pp. 153–168, 2018. doi: 10.1016/j.ymssp.2017.12.014

[8] H. Feng, C. Yin, W. Ma, H. Yu, and D. Cao, "Parameters identification and trajectory control for a hydraulic system," *ISA Transactions*, vol. 92, pp. 228–240, 2019. doi: 10.1016/j.isatra.2019.02.022

[9] Y. Li and Q. Wang, "Adaptive neural finite-time trajectory tracking control of hydraulic excavators," *Proceedings of the Institution of Mechanical Engineers, Part I: Journal of Systems and Control Engineering*, vol. 232, no. 7, pp. 909–925, 2018. doi: 10.1177/0959651818767770

[10] J. Park, B. Lee, S. Kang, P. Y. Kim, and H. J. Kim, "Online learning control of hydraulic excavators based on echo-state networks," *IEEE Transactions on Automation Science and Engineering*, vol. 14, no. 1, pp. 249–259, 2017. doi: 10.1109/TASE.2016.2582213

[11] M. Lee, H. Choi, C. Kim, J. Moon, D. Kim, and D. Lee, "Precision Motion Control of Robotized Industrial Hydraulic Excavators via Data-Driven Model Inversion," *IEEE Robotics and Automation Letters*, vol. 7, no. 2, pp. 1912–1919, 2022. doi: 10.1109/LRA.2022.3142389

[12] P. Egli and M. Hutter, "A general approach for the automation of hydraulic excavator arms using reinforcement learning," *IEEE Robotics and Automation Letters*, vol. 7, no. 2, pp. 5679–5686, 2022. doi: 10.1109/LRA.2022.3152865

[13] H. Feng, Q. Song, S. Ma, W. Ma, C. Yin, D. Cao, and H. Yu, "A new adaptive sliding mode controller based on the RBF neural network for an electro-hydraulic servo system," *ISA Transactions*, 2022. doi: 10.1016/j.isatra.2021.12.044

[14] Y. Yamamoto, J. Qiu, Y. Munemasa, T. Doi, T. Nanjo, K. Yamashita, and R. Kikuuwe, "A sliding-mode set-point position controller for hydraulic excavators," *IEEE Access*, vol. 9, pp. 153 735–153 749, 2021. doi: 10.1109/ACCESS.2021.3128215

[15] R. Kikuuwe, T. Okada, H. Yoshihara, T. Doi, T. Nanjo, and K. Yamashita, "A nonsmooth quasi-static modeling approach for hydraulic actuators," *ASME Journal of Dynamic Systems, Measurement, and Control*, vol. 143, no. 12, p. 121002, 2021. doi: 10.1115/1.4051894

[16] J. E. Normey-Rico and E. F. Camacho, *Control of dead-time processes*. Springer, 2007. ISBN 978-1-84628-828-9 978-1-84628-829-6

[17] M. H. Nguyen, H. V. Dao, and K. K. Ahn, "Extended sliding mode observer-based high-accuracy motion control for uncertain electro-hydraulic systems," *International Journal of Robust and Nonlinear Control*, vol. 33, no. 2, pp. 1351–1370, 2023. doi: 10.1002/rnc.6421

[18] J. Xu and H.-S. Yoon, "Sliding mode control of hydraulic excavator for automated grading operation," *SAE International Journal of Commercial Vehicles*, vol. 11, no. 2, pp. 113–124, 2018. doi: 10.4271/02-11-02-0010

[19] R. Kikuuwe, S. Yasukouchi, H. Fujimoto, and M. Yamamoto, "Proxy-based sliding mode control: a safer extension of PID position control," *IEEE Transactions on Robotics*, vol. 26, no. 4, pp. 670–683, 2010. doi: 10.1109/TRO.2010.2051188

[20] R. Kikuuwe, "A sliding-mode-like position controller for admittance control with bounded actuator force," *IEEE/ASME Transactions on Mechatronics*, vol. 19, no. 5, pp. 1489–1500, 2014. doi: 10.1109/TMECH.2013.2286411

[21] W. Borutzky, B. Barnard, and J. Thoma, "An orifice flow model for laminar and turbulent conditions," *Simulation Modelling Practice and Theory*, vol. 10, no. 3-4, pp. 141–152, 2002. doi: 10.1016/S1569-190X(02)00092-8

[22] K. Kim, M. Kim, D. Kim, and D. Lee, "Modeling and velocity-field control of autonomous excavator with main control valve," *Automatica*, vol. 104, pp. 67–81, 2019. doi: 10.1016/j.automatica.2019.02.041

[23] D. Cristofori and A. Vacca, "Modeling hydraulic actuator mechanical dynamics from pressure measured at control valve ports," *Proceedings of the Institution of Mechanical Engineers, Part I: Journal of Systems and Control Engineering*, vol. 229, no. 6, pp. 541–558, 2015. doi: 10.1177/0959651814568366

[24] A. Lichtarowicz, R. K. Duggins, and E. Markland, "Discharge coefficients for incompressible non-cavitating flow through long orifices," *Journal of Mechanical Engineering Science*, vol. 7, no. 2, pp. 210–219, 1965. doi: 10.1243/JMES_JOUR_1965_007_029_02

[25] Y. Ye, C.-B. Yin, X.-D. Li, W.-J. Zhou, and F.-F. Yuan, "Effects of groove shape of notch on the flow characteristics of spool valve," *Energy Conversion and Management*, vol. 86, pp. 1091–1101, 2014. doi: 10.1016/j.enconman.2014.06.081

[26] D. Wu, R. Burton, and G. Schoenau, "An empirical discharge coefficient model for orifice flow," *International Journal of Fluid Power*, vol. 3, no. 3, pp. 13–19, 2002. doi: 10.1080/14399776.2002.10781143

[27] R. Kikuuwe, Y. Yamamoto, and B. Brogliato, "Implicit implementation of nonsmooth controllers to nonsmooth actuators," *IEEE Transactions on Automatic Control*, vol. 67, no. 9, pp. 4645–4657, 2022. doi: 10.1109/TAC.2022.3163124

[28] H. K. Khalil, *Nonlinear systems*, 3rd ed. Prentice Hall, 2002. ISBN 978-0-13-067389-3

[29] R. Kikuuwe, N. Takesue, A. Sano, H. Mochiyama, and H. Fujimoto, "Admittance and impedance representations of friction based on implicit Euler integration," *IEEE Transactions on Robotics*, vol. 22, no. 6, pp. 1176–1188, 2006. doi: 10.1109/TRO.2006.886262

[30] R. Kikuuwe, T. Okada, H. Yoshihara, T. Doi, T. Nanjo, and K. Yamashita, "Nonsmooth quasistatic modeling of hydraulic actuators," *arXiv:2102.11381*, 2021. doi: 10.48550/arXiv.2102.11381